JACS
JOURNAL OF THE AMERICAN CHEMICAL SOCIETY
Article
pubs.acs.org/JACS

Exploitation of Long-Lived ^{3}IL Excited States for Metal–Organic Photodynamic Therapy: Verification in a Metastatic Melanoma Model

Richard Lincoln,[†] Lars Kohler,[‡] Susan Monro,[†] Huimin Yin,[†] Mat Stephenson,[†] Ruifa Zong,[‡] Abdellatif Chouai,[‡] Christopher Dorsey,[‡] Robie Hennigar,[†] Randolph P. Thummel,*[,‡] and Sherri A. McFarland*[,†]

[†]Department of Chemistry, Acadia University, Wolfville, Nova Scotia B4P 2R6, Canada

[‡]Department of Chemistry, University of Houston, Houston, Texas 77204–5003, United States

Supporting Information

ABSTRACT: Members of a family of Ru(II)-appended pyrenylethynylene dyads were synthesized, characterized according to their photophysical and photobiological properties, and evaluated for their collective potential as photosensitizers for metal–organic photodynamic therapy. The dyads in this series possess lowest-lying ^{3}IL-based excited states with lifetimes that can be tuned from 22 to 270 μs in fluid solution and from 44 to 3440 μs in glass at 77 K. To our knowledge, these excited-state lifetimes are the longest reported for Ru(II)-based dyads containing only one organic chromophore and lacking terminal diimine groups. These excited states proved to be extremely sensitive to trace amounts of oxygen, owing to their long lifetimes and very low radiative rates. Herein, we demonstrate that ^{3}IL states of this nature are potent photodynamic agents, exhibiting the largest photocytotoxicity indices reported to date with nanomolar light cytotoxicities at very short drug-to-light intervals. Importantly, these new agents are robust enough to maintain submicromolar PDT in pigmented metastatic melanoma cells, where the presence of melanin in combination with low oxygen tension is known to compromise PDT. This activity underscores the potential of metal–organic PDT as an alternate treatment strategy for challenging environments such as malignant melanoma.

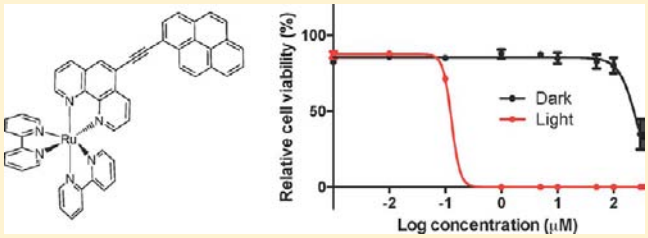

1. INTRODUCTION

1.1. New Approaches to Photosensitizer Design for PDT. Cisplatin, arguably the most successful anticancer drug to date, remains one of the most widely used chemotherapeutic strategies, despite its dose-limiting systemic toxicity and debilitating, long-term side effects. Photodynamic therapy (PDT), a method for destroying unwanted cells and tissue, represents a powerful alternative for treating cancer, alone or in combination with other therapies such as chemo- and immunotherapies, radiation, and surgery. Briefly, PDT overcomes the limitations that plague conventional chemotherapeutics by employing a relatively nontoxic prodrug that becomes toxic only when activated by light. Traditionally, PDT is mediated by singlet oxygen ($^1\Delta_g$), which is produced via excited-state energy transfer from a photosensitizer (PS) to ground state molecular oxygen ($^3\sum_g^-$) in what is known as a primary type II photoprocess. Other photoprocesses can occur, and certainly do, but the general consensus in the field is that singlet oxygen ($^1O_2$) plays a dominant role and is a potent cytotoxic agent in sufficiently oxygenated tissue. Light-activated production of $^1O_2$ ensures that tissue damage is localized only to the region of irradiation. This degree of spatial and temporal selectivity, which can be fine-tuned by judicious choice of the PS, exciting wavelength, and power/energy density, offers all of the advantages of highly targeted therapy (without the cost) with the breadth and scope of classical chemotherapy (without the side effects).

Despite the enormous potential that PDT presents for cancer therapy, in the 40 years since its first use in oncology, it has become neither widely known nor generally accepted as a powerful alternative to existing mainstream approaches, except in a few highly specialized areas of medicine such as dermatological oncology and opthamology. Plaetzer et al.[1] have provided very convincing reasons for the absence of PDT in mainstream cancer treatment modalities, which include (i) the sheer number of variables that must be optimized (PS, drug dose, light source, light dose, drug-to-light interval, dosimetry, and protocol) for each particular clinical application, (ii) the paucity of detailed protocols available to clinicians for existing PDT agents and tumor types, and (iii) the fact that large, controlled, comparative randomized clinical trials have either not been carried out or could not prove significant advantage over existing therapies for advanced cancers that are refractory to other treatments. At some level, each one of these reasons can be linked to the pervasive PS-based approach to drug discovery for PDT, whereby researchers continue to chase the proverbial *ideal* PDT agent with no foresight regarding the

Received: August 14, 2013
Published: October 15, 2013

   dx.doi.org/10.1021/ja408426z | J. Am. Chem. Soc. 2013, 135, 17161–17175

specific application or clinical setting in which PDT will be delivered. In order to exploit the full potential that PDT has to offer, researchers must recognize that *there is no single ideal PS for all PDT applications* and, thus, shift from a PS-centered approach to a tumor-centered approach, which will require working closely with clinicians, cancer biologists, and medical biophysicists. Equal attention must be paid to (i) the PS and proper dosimetry of the PS, light fluence, and oxygen supply in the tumor, (ii) the specific tumor type, application, and clinical setting, and (iii) the development of complete treatment *packages* that include the PS, light source, and detailed protocol.

To date the PS-based approach has focused mainly on PDT agents that absorb red light, with significant effort toward developing improved agents that can be activated in the PDT window (700−900 nm), a range that maximizes tissue penetration while maintaining sufficient energy for $^1O_2$ production. These qualities have long been touted as must-have properties of the ideal PS, although more recently, the ideal PS must exhibit an oxygen-independent mechanism of action for treating hypoxic tissue. When researchers move toward a tumor-centered approach, the ideal PS properties (along with its light source and protocol) will be defined by the tumor type and clinical application. For example, a superficial tumor that is well oxygenated does not demand a near-IR PDT agent that functions in hypoxia for the same reason that a deep tumor isolated from the primary vasculature will not benefit from a blue PDT agent with unity production of $^1O_2$. Herein, we outline the first steps toward implementing this tumor-centered approach in our own laboratories, whereby we provide proof of principle that blue/green-absorbing PDT agents with extremely long excited-state lifetimes of ^{3}IL character yield the largest reported photocytotoxicity indices (PIs) in a standard HL60 cancer cell line. Furthermore, these agents are capable of destroying melanocytes with metastatic potential, enabling PDT in pigmented melanoma cell lines that have traditionally proven less responsive to PDT.[2]

1.2. ^{3}IL States for Metal−Organic PDT. $[Ru(bpy)_3]^{2+}$ and its numerous derivatives remain the subject of intense research effort, owing to a combination of favorable absorption, photophysical, and electrochemical properties.[3] As part of supramolecular systems, they are rivaled only by porphyrin and metalloporphyrins as active components for photoinduced energy and electron transfer.[4] While the ^{3}MLCT-based excited state of $[Ru(bpy)_3]^{2+}$ is considered to be relatively long at 1 μs in deoxygenated solution at room temperature, it is still too short for many luminescence-based applications but does offer a handle for improvement owing to its modular scaffold. Castellano et al.[5] and others[6] have recognized and predicted the importance of instilling even longer excited-state lifetimes in Ru(II) complexes for potential applications in optoelectronics and luminescence-based technologies, and we have shown previously that such properties are also ideal for photobiological applications, particularly PDT.[7] Consequently, considerable effort has been expended toward prolonging the excited-state lifetimes in Ru(II) diimine and other metal-based coordination complexes.[4]

Most approaches start from the basic premise that ^{3}MLCT lifetimes of Ru(II) polypyridine complexes are set by a fundamental interaction between the lowest energy ^{3}MLCT state and a higher-lying ^{3}MC state.[3,8] From this assumption, it follows that ^{3}MLCT lifetimes can be extended by either raising the energy of the ^{3}MC state or lowering the energy of the ^{3}MLCT state, effectively controlling k_{nr} but not necessarily k_r. An alternate approach involves utilization of a spatially separated polycyclic aromatic hydrocarbon, a purely organic chromophore with photophysical properties distinct from the Ru(II) core, to provide a low-lying $^3\pi\pi^*$ state in close energetic proximity to the metal-centered ^{3}MLCT state. Incorporation of organic chromophores into diimine ligand architectures in order to impart novel photophysical characteristics to Ru(II) coordination complexes is a strategy first reported by Ford and Rogers in 1992 to extend excited-state lifetimes.[9] The resulting constructs—termed *dyads*—place the Ru(II)-based ^{3}MLCT excited state in equilibrium with a lowest-lying, long-lived triplet state contributed by the organic unit. The consequence of this bichromophoric arrangement and the existence of quasi-isoenergetic ^{3}MLCT and ^{3}IL states is the creation of an excited-state energy reservoir that prolongs the ^{3}MLCT emission. In this early example, the ^{3}MLCT lifetime was extended over 10-fold, from 0.8 to 11.2 μs. Following this principle with judicious modification of the diimine ligand and organic chromophore, ^{3}MLCT lifetimes in excess of 50 μs have been obtained.[4] Since this pioneering work, subsequent accounts have demonstrated that subtle structural modifications can switch the photophysics from an equilibrium between ^{3}MLCT and ^{3}IL states to pure ^{3}IL or mixed ^{3}IL/^{3}ILCT phosphorescence at room temperature in fluid solution. When the ^{3}IL states of the organic chromophore are much lower in energy than the lowest-lying ^{3}MLCT states, pure ^{3}IL phosphorescence dominates and lifetimes can exceed 150 μs.[4,5,10] Achieving lifetimes of this magnitude in a Ru(II) polypyridyl complex is fascinating from a theoretical perspective but, moreover, presents enormous potential for the use of such photosensitizers in photobiological applications.

In complexes of the type $[Ru(LL')_3]^{2+}$ and $[Ru(LL')_2(bpy)]^{2+}$, where LL′ = 5-(pyren-1-yl)ethynyl-2,2′-bipyridine, the combination of the alkyne linkage with 5-substitution on the 2,2′-bipyridine ring leads to low-lying pure ^{3}IL excited states with lifetimes of 53.1 and 54.3 μs, respectively.[5,10] The related $[Ru(bpy)_2(LL')]^{2+}$ also displays a long lifetime of 42 μs, but the emission spectrum suggests an excited-state equilibrium between ^{3}MLCT and ^{3}IL states (favoring the latter) rather than pure ^{3}IL phosphorescence.[11] From detailed studies of these and similar systems reported in the literature, we reasoned that it should be possible to design a $[Ru(bpy)_2(LL')]^{2+}$ construct with a pure lowest-lying ^{3}IL state by employing 1,10-phenanthroline (phen) as the coordinating ligand instead of 2,2-bipyridine (bpy). This structural change was made on the basis that a related system using phen directly attached to pyrene positions the ^{3}IL state as the dominant state at 77 K.[12] We hypothesized that the ethynylene linker would drop the ^{3}IL state to an even lower energy, allowing pure ^{3}IL phosphorescence at room temperature without the need for two or three pyrenyl units which would decrease water solubility, an important consideration for biological applications. Systems where ^{3}IL or ^{3}IL/^{3}ILCT states dictate the excited-state dynamics and lie at suitably low energy offer the unique opportunity to simultaneously prolong the excited-state lifetime and drastically reduce k_r. Such excited states have been shown to be almost 175× more susceptible to oxygen quenching by comparison to ^{3}MLCT states, with greater than 75% of these ^{3}IL-based states remaining quenched even in hypoxia (3.5% O_2).[13] Such behavior by a photosensitizer presents a new avenue for maintaining potent photobiological activity at low oxygen tension, a significant challenge for PDT that severely limits its utility and scope. In order to demonstrate the robustness of these dyads as PDT agents under the most

challenging conditions, we present the in vitro PDT activity of these dyads in the metastatic melanoma line Malme-3M. This model of melanotic melanoma is characterized by low oxygen saturation and the ability not only to resist but to detoxify ROS, effectively mitigating the effects of conventional type II PDT agents. This investigation was carried out with a Malme-3M population actively producing visible concentrations of melanin, which competes with the photosensitizer for absorption of incoming light, neutralizes ROS, and further depletes oxygen (pO_2 <2% and <0.5% during peak melanin production),[14] conditions that also describe in vivo melanomas.

It has been noted by others[5] that very minor structural modifications can alter the relative energies of MLCT and IL states to such an extent that the observed photophysics can transform toward either extreme. Therefore, in the present investigation, we outline a family of dyads based on the aforementioned design whereby the position of the pyrenyl-ethynylene linker was systematically varied and in one case compared to its related $[Ru(LL')_3]^{2+}$ homoleptic counterpart. The goals were to document the photophysical properties of these dyads as a function of structure, to demonstrate the utility of such dyads as PDT agents under challenging conditions, to underscore the role that PDT may be able to fill in new treatment strategies for advanced melanoma, and to determine whether the minor structural changes probed significantly alter the photobiological activities of these complexes in cells.

2. EXPERIMENTAL PROCEDURES

2.1. Materials. Acetonitrile used for cyclic voltammetry measurements was dried over CaH_2 and freshly distilled prior to use. The 4-bromo-1,10-phenanthroline,[15] 5-bromo-1,10-phenanthroline,[16] 5-ethynyl-1,10-phenanthroline (**5-EP**),[17] $[Ru(DMSO)_4Cl_2]$,[18] and $[Ru(bpy)_2Cl_2]\cdot 2H_2O$[19] were prepared according to known procedures, and 1-ethynylpyrene was purchased from Alfa Aesar and used without further purification. The purified complexes were isolated as PF_6 salts and subsequently subjected to anion metathesis on Amberlite IRA-410 with methanol to yield the more water-soluble Cl salts for biological experiments. Characterized fetal bovine serum (FBS) and Iscove's Modified Dulbecco's Medium (IMDM) supplemented with 4 mM L-glutamine were purchased from Fisher Scientific, and human promyelocytic leukemia cells (HL60) and metastatic melanoma cells (Malme-3M) were procured from the American Type Culture Collection. Prior to use FBS was divided into 40 mL aliquots that were heat inactivated (30 min, 55 °C) and subsequently stored at −10 °C. Water for biological experiments was deionized to a resistivity of 18 MΩ cm using a Barnstead filtration system. Chart 1 gives the formulas for **1**−**5**.

*2.1.1. 5-(Phenylethynyl)-1,10-phenanthroline (**5-BEP**).* In a pressure tube were added 5-bromo-1,10-phenanthroline (300 mg, 1.16 mmol), phenylacetylene (237 mg, 2.32 mmol), $Pd(PPh_3)_4$ (134 mg, 0.116 mmol), and *n*-propylamine (25 mL). After heating at 80 °C for 2 days, the reaction mixture was concentrated, quenched with water, and extracted with CH_2Cl_2. The organic layer was washed with water and brine, dried over $MgSO_4$, and filtered. Chromatography on silica, with CH_2Cl_2/MeOH (3%) as eluent, and recrystallization from diethyl ether afforded **5-BEP** as an off-white solid (195 mg, 60%): mp 127 °C; ^{1}H NMR ($CDCl_3$) δ 9.27 (dd, 1H, J = 4.6, 1.7 Hz), 9.22 (dd, 1H, J = 4.6, 1.7 Hz), 8.87 (dd, 1H, J = 8.0, 1.7 Hz), 8.27 (dd, 1H, J = 8.0, 1.7 Hz), 8.12 (s, 1H), 7.77 (dd, 1H, J = 8.3, 4.0 Hz), 7.70−7.65 (m, 3H), 7.46−7.42 (m, 3H). These NMR data agree with the reported spectrum.[20]

*2.1.2. 4-(Pyren-1-ylethynyl)-1,10-phenanthroline (**4-PEP**).* In a pressure tube were added 4-bromo-1,10-phenanthroline (0.110 g, 0.42 mmol), 1-ethynylpyrene (0.145 g, 0.64 mmol), $Pd(PPh_3)_4$ (0.073 g, 0.06 mmol), and *n*-propylamine (17.6 mL). The tube was sealed and the mixture heated at 80 °C for 2 days. After this time, a yellow precipitate formed, which was filtered and washed with water (10 mL), EtOH (10 mL), and CH_2Cl_2 (10 mL) to afford **4-PEP** (0.075 g, 44%) as a yellow solid: mp 286−288 °C; ^{1}H NMR ($CDCl_3$) δ 9.24 (apparent d, 2 H, J = 4.6 Hz), 8.76 (d, 1H, J = 9.2 Hz), 8.61 (d, 1H, J = 8.7 Hz), 8.05−8.38 (overlapping m, 9H), 7.97 (m, 2H), 7.68 (dd, 1H, J = 8.2, 4.1 Hz). A ^{13}C NMR spectrum could not be obtained due to poor solubility.

*2.1.3. $[Ru(bpy)_2(5\text{-}EP)](PF_6)_2$ (**1**).* The reaction of 5-ethynyl-1,10-phenanthroline (**5-EP**; 30 mg, 0.15 mmol) and $[Ru(bpy)_2Cl_2]\cdot 2H_2O$ (78 mg, 0.15 mmol) in refluxing EtOH/H_2O (13 mL, 10/3) for 2 days gave a red solution. A saturated KPF_6 solution was added, and the solvents were evaporated. The residue was purified by chromatography on alumina with acetone as eluent. The first red fraction was collected and recrystallized from acetone/water to give **1** as an orange powder (90 mg, 63%): ^{1}H NMR (acetone-d_6) δ 8.96 (dd, 1H, J = 8.4, 1.2 Hz), 8.87−8.78 (m, 5H), 8.66 (s, 1H), 8.50 (ddd, 2H, J = 9.0, 5.4, 0.9 Hz), 8.28−8.22 (m, 2H), 8.17−8.12 (m, 4H), 8.01 (dd, 1H, J = 8.1, 5.4 Hz), 7.97−7.91 (m, 3H), 7.65−7.60 (m, 2H), 7.40−7.36 (m, 2H), 4.55 (s, 1H).

*2.1.4. $[Ru(bpy)_2(5\text{-}BEP)](PF_6)_2$ (**2**).* A mixture of 5-(phenylethynyl)-1,10-phenanthroline (**5-BEP**; 50 mg, 0.178 mmol) and $[Ru(bpy)_2Cl_2]\cdot 2H_2O$ (77.3 mg, 0.149 mmol) in EtOH/H_2O (10 mL, 10/3) was heated at reflux for 14 h. The solvent was evaporated; the residue was suspended in water, and the unreacted ligand was removed by extraction with CH_2Cl_2. NH_4PF_6 (400 mg) dissolved in water (3 mL) was added to the aqueous layer. The precipitate was filtered, washed with water, and dried. Recrystallization from acetone/water afforded **2** as an orange solid (132 mg, 90%): ^{1}H NMR (acetone-d_6) δ 9.17 (dd, 1H, J = 8.0, 1.2 Hz), 8.88 (dd, 2H, J = 8.0, 2.9 Hz), 8.86−8.81 (m, 3H), 8.69 (s, 1H), 8.53 (dd, 1H, J = 5.2, 1.2 Hz), 8.48 (dd, 1H, J = 5.4, 1.2 Hz), 8.31−8.25 (m, 2H), 8.22−8.14 (m, 4H), 8.04 (dd, 1H, J = 8.6, 5.2 Hz), 7.99−7.94 (m, 3H), 7.80−7.76 (m, 2H), 7.68−7.65 (m, 2H), 7.57−7.51 (m, 3H), 7.44−7.39 (m, 2H). These NMR data agree with the reported spectrum.[21]

*2.1.5. $[Ru(bpy)_2(5\text{-}PEP)](PF_6)_2$ (**3**).* The complex was prepared in a manner similar to that for its bpy-d_8 analogue.[7] A mixture of 5-pyren-1-ylethynyl-1,10-phenanthroline[7] (**5-PEP**; 40 mg, 0.10 mmol) and $[Ru(bpy)_2Cl_2]\cdot 2H_2O$ (55 mg, 0.10 mmol) in EtOH (15 mL) was refluxed overnight. NH_4PF_6 (180 mg) was added, and the precipitate was collected by filtration. Purification was achieved by chromatography on alumina, with acetone and MeOH/acetone (5%) as eluents. The solvents were evaporated to give **3** as a red solid (92 mg, 83%): ^{1}H NMR (acetone-d_6) δ 9.36 (dd, 1H, J = 8.2, 1.4 Hz), 8.94 (s, 1H), 8.90−8.84 (m, 5H), 8.81 (d, 1H, J = 9.2 Hz), 8.56 (dd, 1H, J = 5.0, 1.4 Hz), 8.51−8.49 (m, 2H), 8.42−8.38 (m, 4H), 8.32 (d, 1H, J = 9.2 Hz), 8.30−8.25 (m, 3H), 8.21−8.15 (m, 5H), 8.11 (dd, 1H, J = 8.2, 5.5 Hz), 8.00−7.97 (m, 3H), 7.67−7.63 (m, 2H), 7.44−7.40 (m, 2H).

*2.1.6. $[Ru(bpy)_2(4\text{-}PEP)](PF_6)_2$ (**4**).* A mixture of 4-(pyren-1-ylethynyl)-1,10-phenanthroline (**4-PEP**; 40 mg, 0.09 mmol) and $[Ru(bpy)_2Cl_2]\cdot 2H_2O$ (0.048 g, 0.1 mmol) in EtOH (25 mL) was refluxed for 18 h under Ar. After the mixture was cooled to room temperature, NH_4PF_6 (saturated aqueous, 3 mL) was added and the solution was stirred for 20 min, concentrated, and purified by chromatography on silica gel, with CH_2Cl_2/MeOH (99/1) as eluent. Recrystallization from acetone/toluene yielded **4** (0.061 g, 56%) as a red-orange solid: ^{1}H NMR (acetone-d_6) δ 8.96 (d, 1H, J = 9.2 Hz),

Chart 1. Ruthenium(II) Dyads (3−5) Based on (Pyren-1-yl)ethynyl Derivatives of 1,10-Phenanthroline and Several Reference Complexes (1, 2)

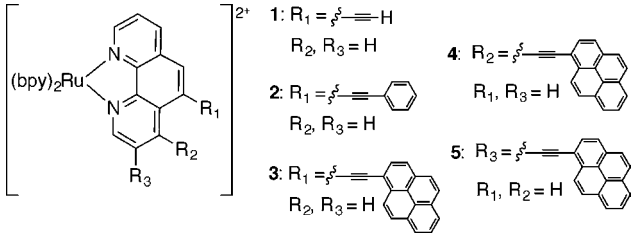

dx.doi.org/10.1021/ja408426z | J. Am. Chem. Soc. 2013, 135, 17161−17175

8.84 (m, 5 H), 8.76 (d, 1H, J = 9.2 Hz), 8.59 (d, 1H, J = 8.7 Hz), 8.51 (m, 3H), 8.33−8.43 (overlapping m, 5H), 8.14−8.30 (overlapping m, 9H), 8.06 (d, 1H, J = 5.0 Hz), 7.92−7.99 (overlapping m, 2H), 7.65 (m, 2H), 7.41 (m, 2H); MS m/z 818 (100%, (M − $2PF_6$)). Anal. Calcd for $C_{50}H_{32}N_6F_{12}P_2Ru{\cdot}CH_2Cl_2$: C, 51.36; H, 2.68; N, 7.05. Found: C, 51.27; H, 2.90; N, 6.77.

*2.1.7. [Ru(bpy)$_2$(3-PEP)](PF$_6$)$_2$ (**5**).* The complex was prepared in a manner similar to that for its bpy-d_8 analogue.[7] A mixture of 3-pyren-1-ylethynyl-1,10-phenanthroline (**3-PEP**; 40 mg, 0.10 mmol) and $Ru(bpy)_2Cl_2{\cdot}2H_2O$ (55 mg, 0.10 mmol) in EtOH (15 mL) was refluxed overnight. NH_4PF_6 (180 mg) was added, and the precipitate was collected by filtration. Purification was achieved by chromatography on alumina, with acetone and a MeOH/acetone (1−5%) mixture as eluents. Evaporation of the solvent gave **5** as a red solid (92 mg, 83%): ^{1}H NMR (acetone-d_6) δ 9.13 (d, 1H, J = 1.8 Hz), 8.90 (d, 1H, J = 8.2 Hz), 8.85 (d, 1H, J = 8.2 Hz), 8.82 (dd, 2H, J = 8.2, 1.4 Hz), 8.81 (d, 1H,J = 8.2 Hz), 8.67 (d, 1H, J = 1.8 Hz), 8.48−8.12 (m, 19H), 7.95 (d, 1H, J = 5.5 Hz), 7.93 (d, 1H, J = 5.5 Hz), 7.72 (ddd, 1H, J = 7.6, 5.7, 1.4 Hz), 7.64 (ddd, 1H, J = 7.6, 5.7, 1.2 Hz), 7.44−7.39 (m, 2H).

*2.1.8. [Ru(5-PEP)$_3$](PF$_6$)$_2$ (**6**).* A mixture of 5-(pyren-1′-ylethynyl)-1,10-phenanthroline (**5-PEP**; 101 mg, 0.25 mmol) and [Ru(DMSO)$_4$Cl$_2$] (40 mg, 0.08 mmol) in 95% EtOH (20 mL) was refluxed under Ar for 24 h. After cooling, NH_4PF_6 (excess) in H_2O (5 mL) was added and the mixture was stirred for 15 min. The solvent was evaporated, and the crude product was filtered through silica gel, with CH_2Cl_2/MeOH (99/1) as eluent. After evaporation of the solvent, an orange solid was obtained which showed some small impurities by ^{1}H NMR. After a second silica gel column was used, with the same solvent mixture as eluent, pure **6** (as a mixture of stereoisomers) was obtained (27 mg, 21%): ^{1}H NMR (CD_3CN) δ 9.24−9.20 (m, 3H), 8.82 (d, 3H, J = 9.2 Hz), 8.77 (s, 1H), 8.77 (s, 1H), 8.76 (s, 1H), 8.66−8.63 (m, 3H), 8.47 (d, 3H, J = 8.2 Hz), 8.40 (d, 3H, J = 9.6 Hz), 8.40−8.33 (m, 9H), 8.27 (d, 3H, J = 9.2 Hz), 8.21−8.10 (m, 12H), 7.86−7.81 (m, 3H), 7.73−7.68 (m, 3H).

2.2. Instrumentation. Nuclear magnetic resonance spectra were recorded at 400 MHz on a JEOL ECX400 NMR spectrometer and referenced to the residual solvent peak for $CDCl_3$, acetone-d_6, or CD_3CN. Electronic absorption spectra were measured on Jasco V-530 and PerkinElmer Lambda 3B spectrophotometers. Emission spectra were obtained on PTI Quantamaster and PerkinElmer LS-50 luminescence spectrometers and have been corrected for instrument response. The PTI Quantamaster was equipped with a standard R928 PMT for measuring conventional emission (<900 nm) and a Hamamatsu R5509-42 near-IR PMT for measuring near-IR emission (<1400 nm). Cyclic voltammetry (CV) experiments were performed at room temperature in a one-compartment cell equipped with a glassy-carbon working electrode, a saturated calomel reference electrode (SCE), and a platinum wire as the auxiliary electrode in CH_3CN containing (n-butyl)$_4$N(PF$_6$) (0.1 M) at a scan rate of 100 mV s^{-1}.[22] Mass spectra were obtained on a Voyager-DE-STR MALDI-TOF mass spectrometer using α-cyano-4-hydroxycinnamic acid as matrix. CHN analyses were performed by Quantitative Technologies Inc., Whitehouse, NJ. Melting points were measured on a Hoover capillary melting point apparatus and are not corrected. Cell counting and imaging were carried out using a Nikon Eclipse TE2000-U inverted light microscope in phase-contrast mode or epi-fluorescence mode (G-2A epi-fluorescence filter block). Manual cell counting was done using a Neubauer hemocytometer (Hausser Scientific) and ESBE Scientific's Cellometer Auto T4 Plus Cell Counting System.

2.3. Methods. *2.3.1. Cell Culture. 2.3.1.1. HL60.* HL-60 human promyelocytic leukemia cells (ATCC CCL-240) were cultured at 37 °C under 5% CO_2 in Hyclone's IMDM, supplemented with 20% FBS and 25 μg mL^{-1} gentamycin sulfate, and were passaged three to four times per week according to standard aseptic procedures. Cultures were started at 200000 cells mL^{-1} in 25 cm^2 tissue culture flasks and were subcultured before growth reached 750000 cells mL^{-1} to avoid senescence associated with prolonged high cell density. Complete media was prepared in 200 mL portions as needed by combining IMDM (160 mL), FBS (40 mL, prealiquoted and heat inactivated), and gentamicin sulfate (100 μL of 50 mg mL^{-1} stock solution) in a 250 mL Millipore vacuum stericup (0.22 μm) and filtering.

2.3.1.2. Malme-3M. Malme-3M cells (ATCC HTB-64) were cultured at 37 °C under 5% CO_2 in OptiMEM I, supplemented with 10% FBS and were passaged two to three times per week according to standard aseptic techniques. Cultures were started at 500000 cells mL^{-1} in 75 cm^2 tissue culture flasks and were subcultured before growth reached 800000 cells mL^{-1} in order to avoid senescence associated with prolonged high cell density and also to maintain the heterogeneity of the mixture. Complete media was prepared in 250 mL portions as needed by combining OptiMEM I (225 mL) and FBS (25 mL, prealiquoted and heat inactivated) in a 250 mL Millipore vacuum stericup (0.22 μm) and filtering.

2.3.2. Cytotoxicity and Photocytotoxicity Assays. 2.3.2.1. HL60. A 200 μL portion of PBS (no Ca or Mg) was added to the outer wells (nonsample wells) of two 96-well microplates to prevent evaporation from inner wells. Then 25 μL of complete cell media was added to each sample well, and the plates were incubated at 37 °C (5% CO_2) for 15 min before adding 50 μL of cell culture (HL-60 cells growing in log phase, approximately 8 × 10^5 cells mL^{-1}) to each sample well. The cells in microplates were incubated for 1 h at 37 °C (5% CO_2). Serial dilutions of each photosensitizer were warmed and then added to the wells containing cell cultures in 25 μL aliquots. The photosensitizer-treated plates were incubated for 1 h (37 °C, 5% CO_2), and this incubation time is referred to as the pre-PDT incubation time. Following the pre-PDT incubation period, the dark plate was left in the incubator, and the light plate was illuminated under a 190 W projector (BenQ MS510) for 1 h without any filters in place (power density 27.8 mW cm^{-2}; energy density 100 J cm^{-2}). Cell loss under these conditions due to light treatment alone is under 10% and generally less than 5%. Both light and dark microplates were then returned to the incubator for 48 h, at which point 10 μL of a 0.1% solution of Alamar Blue in PBS was added to each well for cell viability determination and left to incubate for an additional 15 h at 37 °C under 5% CO_2. Total post-PDT incubation time was approximately 63 h. A Cytofluor 4000 fluorescent microplate reader was used to count the number of viable cells indicated by fluorescence from the Alamar Blue metabolized byproduct using a 530/25 nm excitation and 620/40 nm emission filter set. EC_{50} values for cytotoxicity were calculated from sigmoidal fits of the dose response curves using Graph Pad Prism 6.0 according to eq 1, where y_i and y_f are the initial and final fluorescence signal intensities, respectively.

$$y = y_i + \frac{y_i - y_f}{1 + 10^{(\log EC_{50}) \times (\text{Hill slope})}} \quad (1)$$

2.3.2.2. Malme-3M. Malme-3 M cells were grown to good visible confluence, typically about 5000−6000 cells/mL, and used without further quantification. A 200 μL portion of PBS (no Ca or Mg) was added to the outer wells (nonsample wells) of two 96-well microplates to prevent evaporation of inner wells. Then 25 μL of complete cell media was added to each sample well, and the plates were incubated at 37 °C (5% CO_2) for 15 min before adding 50 μL of cell culture to each sample well. The cells in microplates were incubated for 1 h at 37 °C (5% CO_2). Serial dilutions of each photosensitizer were warmed and then added to the wells containing cell culture in 25 μL aliquots. The photosensitizer-treated plates were incubated for 1 h (37 °C, 5% CO_2), and this incubation time is referred to as the pre-PDT incubation time. Following the pre-PDT incubation period, the dark plate was left in the incubator, and the light plate was illuminated in a Luzchem photoreactor for 15 min using visible fluorescent bulbs (power density 7.67 mW cm^{-2}; energy density 6.9 J cm^{-2}). Both light and dark microplates were then returned to the incubator for 48 h, at which point 10 μL of a 0.1% solution of Alamar Blue in PBS was added to each well for cell viability determination according to the methods described for HL60 cells.

2.3.3. Spectroscopic Methods. All photophysical studies were conducted on dilute (10^{-6}−10^{-5} M) solutions prepared in spectroscopic-grade solvents. Oxygen was removed from room

Table 1. Cyclic Voltammetry Data for Several Reference Compounds and the Ru(II) Dyads Used in This Study

		$E_{1/2}^{red}$ (ΔE)[a]		
compd	$E_{1/2}^{ox}$ (ΔE_p)[a]			
$[Ru(bpy)_2(phen)](PF_6)_2$	+1.27 (74)[b]	−1.36 (77)[b]	−1.55 (84)[b]	−1.79 (86)[b]
1	+1.28 (74)	−1.28[ir]	−1.54[ir]	
2	+1.29 (86)	−1.28[ir]	−1.53[ir]	
3	+1.32 (128)[b]	−1.11[ir b]	−1.48 (98)[b]	−1.81[ir b]
4	+1.33 (60)	−1.31[ir]	−1.48 (51)	−1.80[ir]
5	+1.31 (107)[b]	−1.21 (79)[b]	−1.45 (107)[b]	−1.81[ir b]

[a]Spectra were recorded in MeCN containing 0.1 M NBu_4PF_6 with a glassy-carbon electrode at a scan rate of 100 mV/s. $E_{1/2} = (E_{pa} + E_{pc})/2$ is reported as V vs SCE and $\Delta E = (E_{pa} - E_{pc})$ in mV. The notation ir denotes an irreversible process, and the value was estimated by differential peaks. [b]Ref 7.

temperature samples by repeated (minimum of three) freeze−pump−thaw cycles in a custom-made cuvette, and measurements were made in vacuo. Frozen samples were prepared by placing a 5 mm i.d. NMR tube of complex (4/1 ethanol/methanol) in a quartz-tipped cold finger Dewar (fabricated by Wilmad Labglass) filled with liquid nitrogen. Quantum yields of emission (Φ_{em}) and singlet oxygen (Φ_Δ) were measured relative to $[Ru(bpy)_3](PF_6)_2$, where Φ_{em}= 0.062 at room temperature in deaerated acetonitrile, Φ_{em}= 0.38 at 77 K in frozen 4/1 v/v ethanol/methanol,[3] and Φ_Δ= 0.57 in aerated acetonitrile.[23] Absorption spectra were recorded with a Jasco V-530 spectrophotometer. Steady-state luminescence spectra were measured on a PTI Quantamaster setup equipped with a K170B PMT for measuring ultraviolet and visible emission and a Hamamatsu R5509-42 near-IR PMT for measuring near-infrared (near-IR) emission (<1400 nm). Short phosphorescence lifetimes (<1 μs) were measured on a PTI LaserStrobe spectrofluorometer with an R928 stroboscopic detector, pumped by a GL-3300 nitrogen/GL-301 dye laser (2−3 nm fwhm). Long phosphorescence lifetimes (>1 μs) and time-resolved emission spectra were recorded on a PTI Quantamaster setup equipped with a gated detector with a xenon flash lamp as the excitation source. Excited-state lifetimes were extracted from the observed data using PTI Felix32 fitting software. Emission and excitation spectra were corrected for the wavelength dependence of lamp output and detector response.

3. RESULTS AND DISCUSSION

3.1. Synthesis. In earlier work we have reported the preparation and study of complexes **3** and **5** having 2,2-bipyridine-d_8 (bpy-d_8) as the auxiliary ligand.[7] The original motive for preparing these bpy-d_8 systems was to aid in their characterization by ^{1}H NMR, since all the bpy signals would be silent and thus assignment of protons on the target ligand would be facilitated. Considering the promising photobiological activities we identified for these two complexes as well as a report from Tor and co-workers on dual emission from similar compounds,[21] we decided to add the 4-substituted isomer to the series as well as prepare protio analogues of the previously studied deutero systems. All the ethynyl-substituted 1,10-phenanthrolines were prepared by a Sonogashira coupling reaction between the appropriate alkyne and the 3-, 4-, or 5-bromo-1,10-phenanthroline. All three of these bromo derivatives had been previously reported,[7,15,16] and the ligands **3-PEP** and **5-PEP** were described in our earlier work.[7] The coupling to form the **4-PEP** ligand proceeded in 44% yield. As models for the **5-PEP** complex, which proved to be the most biologically active system, we also prepared the previously reported 5-ethynyl-[17] and 5-phenylethynyl-1,10-phenanthrolines by straightforward Sonogashira methodology. Complexes **1**−**5** were prepared by treating the appropriate ligand with 1 equiv of $[Ru(bpy)_2Cl_2]\cdot 2H_2O$. Although the ethynylphenanthrolines are unsymmetrical, the resulting complexes were formed as a single geometric isomer existing as Δ/Λ stereoisomers. The complexes **1** and **2** had been reported earlier.[21,24] All of the complexes were characterized by their ^{1}H NMR spectra, which showed generally well resolved first-order behavior and are included as Figures S1−S8 (Supporting Information). Again because of the apparent importance of the 5-substituted system, we also prepared the homoleptic complex $[Ru(\mathbf{5\text{-}PEP})_3](PF_6)_2$ by treating **5-PEP** with 0.33 equiv of $[Ru(DMSO)_4Cl_2]$. Since the **5-PEP** ligand is unsymmetrical, the tris complex was formed as facial and meridional geometric isomers. These isomers are evidenced in the ^{1}H and ^{1}H−^{1}H COSY NMR spectra. The peaks at 8.77−8.76 ppm do not correlate with any other peaks in the COSY spectrum, indicating that they are all, in fact, singlets attributable to the H6 proton of **5-PEP** in different environments. The protons H2/H9 at 9.22/8.65 ppm and H3/H8 at 7.83/7.71 ppm appear as complicated multiplets, well isolated and identified by the COSY spectrum. The H4/H7 protons resonate in the region 8.22−8.10 ppm, overlapping with pyrene signals. Because of the magnetic anisotropy of the underlying ligand,[25] the H2/H9 protons are separated by 0.57 ppm while only 0.12 ppm separates the H3/H8 protons. The doublets at 8.82 and 8.47 ppm are due to pyrene H2′ and H10′ being closer to the ethynyl bridge.

3.2. Electrochemistry. The half-wave redox potentials for this family of photosensitizers were determined by cyclic voltammetry in acetonitrile solution and are compiled in Table 1. For a typical Ru(II) polypyridyl complex, the oxidation wave is generally associated with the removal of an electron from a metal dπ orbital. Such an oxidation would normally be favored by electron-donating ligands. The fact that the oxidation potentials for **1** and **2** were nearly identical with that of the parent complex $[Ru(bpy)_2(phen)]^{2+}$ suggests that ethynyl or phenylethynyl substitution has only a slight effect on the $Ru^{II/III}$ process. Changing this substituent to a pyren-2-ylethynyl group made oxidation slightly less favorable, raising the oxidation potential by about 0.05 V.

The observed reduction potential is associated with the addition of an electron, normally to the π* orbital of the most electronegative ligand. For the parent complex, three distinct and reversible waves were observed, corresponding to the successive addition of an electron to each of the three ligands. For some complexes the third wave was irreversible and sometimes hard to distinguish. The nearly identical reduction potentials for **1** and **2** again indicated that the electronic difference between an ethynyl and a phenylethynyl substituent is small. There was a difference of 0.10 V between the first reduction potentials of **3**−**5**, with **3** being the easiest to reduce and **4** being the most difficult. For all three complexes, the second and third reductions were nearly identical and most

dx.doi.org/10.1021/ja408426z | J. Am. Chem. Soc. 2013, 135, 17161−17175

likely involve the addition of an electron to the auxiliary 2,2′-bipyridine ligand.

3.3. Photophysical Properties. *3.3.1. Absorption.* The longest wavelength absorption maxima of dyads **3**−**5** as well as the corresponding homoleptic analogue of **3**, compound **6**, are compared to the prototype $[Ru(bpy)_3]^{2+}$ in Table 2. Typical $^1\pi\pi^*$ ligand-centered transitions of varying intensities but similar to the parent $[Ru(bpy)_2(phen)]^{2+}$ complex in energy were observed in the UV portion of the spectra below 220 nm and near 280 nm for all three dyads (Figure 1a). These electronic transitions as well as the intervening high-energy ^{1}MLCT transitions at 230−240 nm are localized on 2,2′-bipyridyl and the 1,10-phenanthroline core. In contrast, the visible absorption observed for all of the dyads contained overlapping contributions from both low-energy ^{1}MLCT transitions of $d\pi \rightarrow \pi^*$ origin (bpy, phen, or substituted phen serving as the LUMO) and $\pi\pi^*$ transitions involving (pyren-1′-yl)ethynyl-1,10-phenanthroline. While steady-state spectroscopy could not distinguish these two types of transitions, a sharp peak surfaced at approximately 382 nm in the spectrum collected for each of the dyads and served as an indicator for the presence of long-wavelength $\pi\pi^*$ transitions centered on the grafted (pyren-1′-yl)ethynyl-1,10-phenanthroline unit.[5] Spectra acquired for the free ligands (Figure 2a) confirmed this assignment. While C3 and C5 substitution of 1,10-phenanthroline with the π-extended pyrenylethynylene chromophore produced qualitatively similar spectra with discernible ^{1}MLCT shoulders near 450 nm and maxima near 412 nm, C4 substitution led to a 70 nm red shift of the longest wavelength absorption maximum in fluid solution (up to 64 nm in glass) relative to dyads **3** and **5**. The diagnostic, localized (pyren-1′-yl)ethynyl-1,10-phenanthroline $\pi\pi^*$ transition at 382 nm observed for **3** and **5** did not shift in the spectrum of **4**, suggesting that C4 substitution on the 1,10-phenanthroline core does not alter the energetics of the ligand-centered transitions significantly. This lack of influence was confirmed by virtually identical absorption spectra of the free ligands for the three positional isomers of the 1,10-phenanthroline unit (Figure 2a). The profound influence that C4 substitution has on the nature of the ^{1}MLCT transition of the metal complex suggests that substitutions made para to the coordinating nitrogen atoms of 1,10-phenanthroline enable increased electronic communication between the pyrenylethynylene chromophore and the Ru(II) center. Consequently, it is possible to shift the absorption profile of the photosensitizer by subtle structural modification at this particular position, thereby extending the window of activation (and possibly observation) in photobiological applications. Importantly, and of biological relevance, this enhanced conjugation for C4 substitution remains substantial in the solid state, as indicated by the absorption spectra collected at 77 K (Table 2).

Table 2. Absorption and Emission Maxima for the Dyads[a]

	298 K (degassed MeCN)		77 K (4/1 EtOH/MeOH glass)		
compd	λ_{abs} (nm)	λ_{em}(max) (nm)	λ_{abs} (nm)	λ_{em}(max) (nm)	ΔE_s (cm^{-1})
3	412	675	421	672	66
4	482	708	485	696	244
5	414	671	421	668	67
6	412	675	421	674	22
$[Ru(bpy)_3]^{2+}$	446	624	448	583	1127

[a]Absorption and emission maxima were reproducible to within ±2 nm.

3.3.2. Emission. At room temperature in aerated MeCN, dyads **3**−**5** and the homoleptic analogue of **3** (complex **6**) were essentially nonemissive ($\Phi_{em} < 0.005$). Argon-sparged samples produced inconsistent luminescence output, underscoring the extreme sensitivity of the dyad emission quantum yields to trace amounts of oxygen. This sensitivity has been exploited by Ji et al. for luminescence oxygen sensing in the case of **5**[13] and was, therefore, not unexpected. Degassing by the freeze−pump−thaw method or cooling to 77 K produced structured, steady-state emission extending from 570 nm into the near-IR with reproducible quantum yields ranging from 0.1 to 2.0% in degassed MeCN and from 3.2 to 6.2% in 4/1 EtOH/MeOH glass (Table 3). Dyads **3** and **5**, substituted with the pyrenylethynylene group at positions 5 and 3 of the 1,10-phenanthroline ring, respectively, produced qualitatively similar emission spectra in deoxygenated MeCN at 298 K that extended slightly past 900 nm (Figure 1b). The peak maxima in the vibronic progression occurred near 671−675, 742−748, and 830 nm in these systems, corresponding to stretching frequencies of approximately 1350−1450 cm^{-1} that are diagnostic of diimine involvement[16] in the emissive excited states. A high-energy shoulder was evident in the spectrum of **3** at 621 nm, the characteristic region for ^{3}MLCT emission from $[Ru(bpy)_3]^{2+}$ and its close relatives, and this transition was much less pronounced in **5** but discernible at 621 nm. In agreement with its absorption properties, the emission

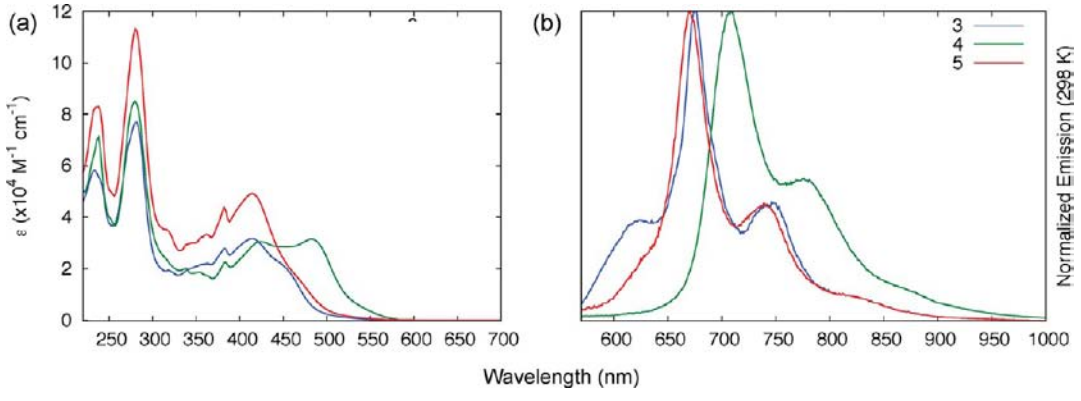

Figure 1. Room-temperature absorption and emission spectra of three positional isomers of the dyads (5 μM, MeCN).

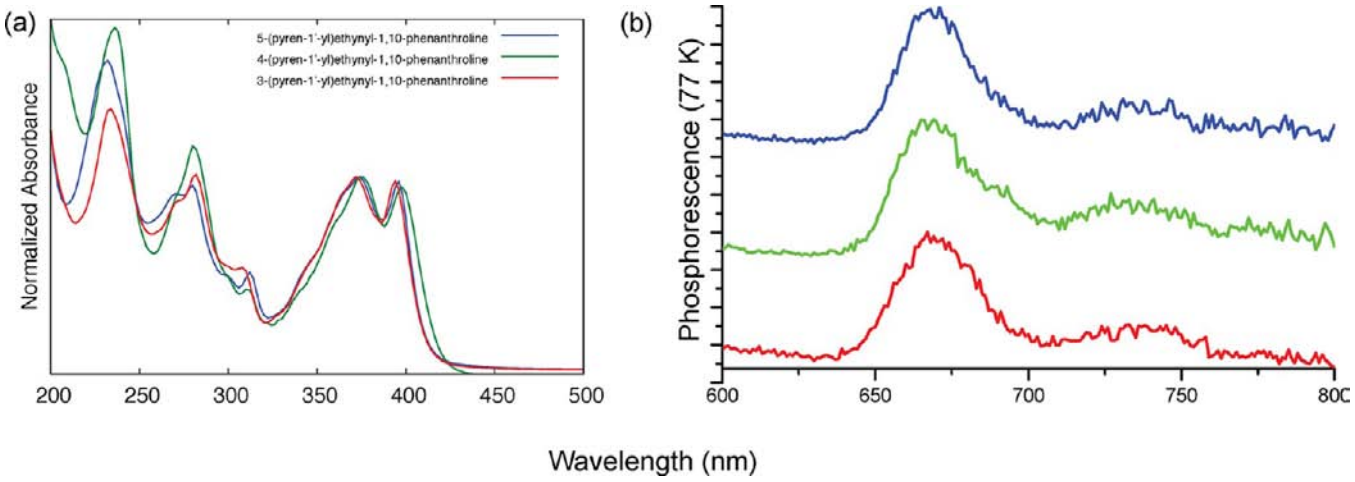

Figure 2. Room -temperature normalized absorption spectra (5 μM, cyclohexane) (a) and ethyl iodide induced phosphorescence at 77 K (20 μM, 4/1 EtOH/MeOH, 10% v/v ethyl iodide) (b) for the free ligands of complexes **3**–**5**.

Table 3. Emission and Singlet Oxygen Quantum Yields for the Dyads[a]

	Φ_{em}		
compd	77 K (4/1 EtOH/MeOH glass)	298 K (degassed MeCN)	Φ $^1O_2$ 298 K (aerated MeCN)[b]
3	0.035	0.0012	0.68
4	0.032	0.018	0.87
5	0.062	0.020	0.65
6	0.020	0.00062	0.67

[a]Quantum yields are an average of at least three measurements and were reproducible to within ±10% for dyad phosphorescence and within ±5% for singlet oxygen phosphorescence. [b]Calculated from direct measurement of $^1O_2$ emission at 1268 nm.

produced by **4** was also red shifted significantly, but with similar vibronic intervals, in comparison to the other dyads. All peaks of the vibronic progression were systematically shifted by 35–40 nm, extending the luminescence output to 1000 nm (Figure 1b). No ^{3}MLCT emission centered near 620 nm was evident in the spectrum collected for **4** at room temperature or at 77 K.

Emission spectra collected at 77 K in 4/1 EtOH/MeOH for complexes **3**–**5** exhibited peak maxima and vibronic fine structure that were narrower than but otherwise similar to those of their room-temperature counterparts, except for the disappearance of the short-wavelength emission near 620 nm that was observed for **3** and **5** in the room-temperature spectra (Figure S10, Supporting Information). The thermally induced Stokes shifts ranged from 66 cm^{-1} for **3** to 244 and 67 and cm^{-1} for **4** and **5**, respectively (Table 2). The onsets of the structured emissions from **6** at room temperature and at 77 K were almost superimposable, producing a thermally induced Stokes shift of only 22 cm^{-1} in the homoleptic analogue of **3**. Under identical conditions, the thermally induced Stokes shift for $[Ru(bpy)_3]^{2+}$ was approximately 1127 cm^{-1} and its room-temperature emission was broad and structureless, in agreement with literature reports and what is expected for polar excited states of ^{3}MLCT character.[10] The small magnitude of the thermally induced Stokes shifts calculated for **3**–**6** in conjunction with their structured emission at room temperature in fluid solution and at 77 K in glass implicates less polar ^{3}IL states as more important contributors to the overall excited-state dynamics in these dyads. Nevertheless, the spread of the thermally induced Stokes shifts within this family points toward ^{3}IL states with different degrees of charge-transfer character, with **6** being most pure, **4** being better assigned as ^{3}IL/^{3}ILCT, and **3** and **5** being somewhat intermediate.

At room temperature and 77 K, **3** and **5** showed 51–55 nm red shifts in the most pronounced vibronic band of their respective progressions relative to the 620 nm maximum for $[Ru(bpy)_3]^{2+}$ ^{3}MLCT emission, and **4** showed an 88 nm red shift at room temperature and only slightly less at 77 K. Taken together, the luminescence data for **3**–**5** suggest photophysics dominated by excited states that are relatively nonpolar and are thus consistent with ^{3}IL $\pi\pi^*$-based emission localized on the pyrenyl unit rather than emission from a low-lying ^{3}MLCT state.[5] The homoleptic analogue of **3**, dyad **6**, produced emission at room temperature and 77 K that was identical with that of **3**, corroborating the assertion that the excited-state dynamics are dominated by transitions involving the pyrenyl chromophoric unit. The ethyl iodide induced phosphorescence observed for the pyrenylethynylene-based free ligands of **3**–**5** (Figure 2b) was similar in structure and energy to the emission produced by Ru(II) dyads **3** and **5**, further supporting lowest-lying ^{3}IL $\pi\pi^*$ states for the complexes. As observed in the absorption spectra, the heavy atom induced phosphorescence at 77 K from 4-pyren-1′-ethynyl-1,10-phenanthroline was not red-shifted relative to the 5- or 3-substituted congeners. However, its complexation to Ru(II) resulted in ^{3}IL-based emission similar in structure but shifted in energy by comparison to **3** and **5**. This larger red shift in the longest wavelength absorption maximum and the room-temperature and 77 K emission was imparted only in the case of 4-pyren-1′-ethynyl-1,10-phenanthroline by coordination to Ru(II) in **4** and indicates that the photophysical properties of these dyads are distinct from ^{3}MLCT states and particularly sensitive to substitution along the coordination axis to the metal center.

3.3.3. Excited State Lifetimes. Excited-state lifetime measurements were attempted on two emission systems with different capabilities: a N_2-dye laser integrated with a stroboscopic detector for lifetimes shorter than 25–30 μs, and a xenon flash lamp and gated detector for phosphorescence lifetimes longer than 1 μs. In fluid solution at room temperature and in glass at 77 K, dual emission was detected for **3** and **5** using gated techniques at wavelengths typical of ^{3}MLCT and ^{3}IL phosphorescence (Figure 3). Regardless of temperature, the

dx.doi.org/10.1021/ja408426z | J. Am. Chem. Soc. 2013, 135, 17161–17175

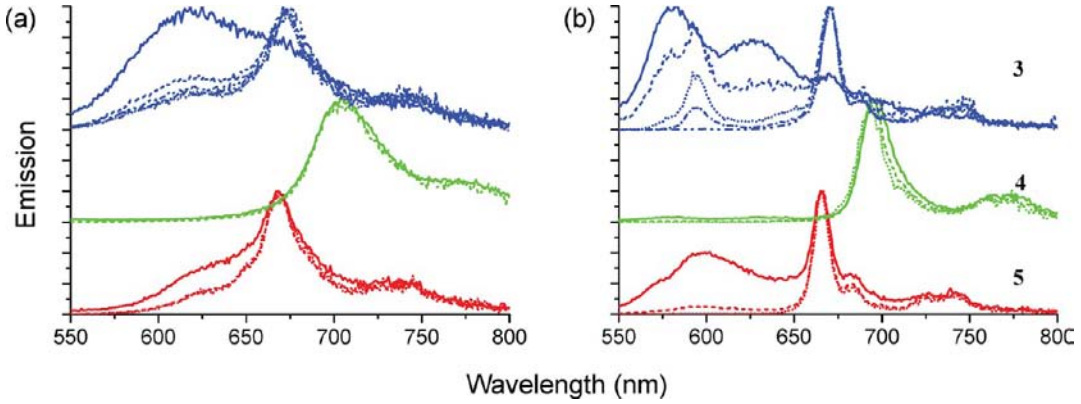

Figure 3. Gated emission for the complexes at 298 K (a) and at 77 K (b). Solid curves represent spectra acquired immediately following the lamp pulse (t = 0, 5 μs gate). Dashed curves represent spectra acquired at progressively longer delay times.

Table 4. Emissive Lifetimes for ^{3}MLCT and ^{3}IL States of the Dyads Compared to the Reference Compound $[Ru(bpy)_3]^{2+}$ [a]

	77 K (4/1 EtOH:/MeOH glass)				298 K (degassed MeCN)			
	^{3}MLCT		^{3}IL		^{3}MLCT		^{3}IL	
compd	λ_{em} (nm)	τ(μs)	λ_{em} (nm)	τ (μs)	λ_{em} (nm)	τ (μs)	λ_{em} (nm)	τ (μs)
3	593	10	670	3430	614	*c*	673	240
4	*b*	*b*	693	44	*b*	*b*	700	22
5	600	7.9	665	330	617	*c*	668	140
6	*b*	*b*	672	3440	*b*	*b*	670	270
$[Ru(bpy)_3]^{2+}$	582	5.1	*b*	*b*	611	0.89	*b*	*b*

[a]Lifetimes represent an average of at least five measurements with uncertainties <10%; data were collected using the corresponding absorption maxima given in Table 1 as the excitation wavelengths (±2 nm). [b]Not detected. [c]Too short to measure.

two dyads produced ^{3}MLCT-like emission near 590−620 nm and ^{3}IL phosphorescence with the onset of maximum vibronic structure beginning near 665−670 nm. These two emissive states were discerned in the steady-state room-temperature spectra in fluid solution as a short-wavelength shoulder overlapping with the longer wavelength structured emission defined by resolved vibronic intervals of diimine stretching modes (Figure 1b). The short-wavelength shoulder has been observed by others,[5] but the overall luminescence from 550 to 850 nm was assigned to one emissive state in this case due to symmetrical quenching of the short- and long-wavelength components by oxygen. In the present series, inefficient deoxygenation of samples hinted that the broad, structureless ^{3}MLCT-like band at shorter wavelengths was quenched less by molecular oxygen than the structured emission at longer wavelengths.

To probe this difference, the gated emission for **3**−**5** was collected at room temperature from 550 to 800 nm at time 0 relative to the lamp pulse with a 5 μs window (Figure 3a, solid curves). While **4**, lacking the ^{3}MLCT band at all times and temperatures investigated, showed an ^{3}IL-based spectrum that did not change notably in the first 5 μs after the lamp pulse, the spectra of **3** and **5** evolved considerably over the first 5 μs after the pulse. **3** showed a much larger contribution of the ^{3}MLCT-based emission at time 0 in comparison to **5**, and **3** was the only dyad where a rise in the ^{3}IL-based phosphorescence might coincide with the decay of the ^{3}MLCT-based emission, although at 5 μs after the lamp pulse the ^{3}MLCT decay was not entirely complete yet the ^{3}IL-based emission was maximal. Unfortunately, the ^{3}MLCT signal was too weak to be detected reliably with nanosecond stroboscopic methods and decayed too quickly to be followed on the gated system. In contrast, the ^{3}IL-based state was clearly established within the lamp pulse for **5** and did not change as the ^{3}MLCT decayed over the first 5 μs. From the gated spectra of **3** and **5**, it appeared that the decay of the ^{3}MLCT band in **3** was marginally slower than in **5**, but both dyads displayed almost identical ^{3}IL-based phosphorescence by 100 μs after the lamp pulse. Interestingly, this ^{3}IL emission profile contained a small shoulder near 625 nm that was symmetrically quenched by oxygen, indicating that this blue shoulder and the onset of structured emission comprised a single emissive state represented by the longer-lived component. The dual emissive behavior for **3** and **5** can be seen very clearly in the gated measurements collected in a glassy matrix at 77 K (Figure 3b). The ^{3}MLCT spectrum of **3** evolved in a complex manner whereby decay of the blue edge (575 nm) of the ^{3}MLCT band occurred very quickly while decay at the red edge (600 nm) occurred much more slowly or perhaps not at all over the first 500 μs after the lamp pulse. Similar to the room-temperature spectra collected for **3**, the ^{3}MLCT-based emission was established within the excitation pulse and dominated at time 0. At 5 μs, ^{3}IL-based emission was established and remained unchanged for more than 1 ms. The behavior of **5** was less complex in that the ^{3}MLCT-based emission had almost completely decayed within the first 5 μs after the pulse. While it is possible that the ^{3}MLCT decay is equally complex in **5**, the dynamics were too short to measure using gated methods and too weak for the nanosecond detection system. Unlike **3**, the ^{3}IL-based emission for **5** was completely established within the excitation pulse and was unaltered by the decay of the shorter ^{3}MLCT-based emission. In contrast to the room-temperature spectra, at 77 K the ^{3}IL-based spectra of **3** and **5** collected after complete decay of the

dx.doi.org/10.1021/ja408426z | J. Am. Chem. Soc. 2013, 135, 17161−17175

^{3}MLCT component did not exhibit a discernible shoulder in this region.

On the nanosecond time scale, emission from the dyads at room temperature or at 77 K did not decay over the observable time window, and contributions from any weakly emitting states with lifetimes less than 1−10 μs were swamped by the longer-lived emission. Consequently, all reported lifetimes were measured using the gated system in an effort to quantify the unusually long decays as well as the shorter decays at different wavelengths. The excited-state lifetimes measured at room temperature and at 77 K for these dyads are given in Table 4 along with the wavelengths at which these lifetimes were monitored. Although the decay of the ^{3}MLCT component for **3** and **5** could be seen in the gated spectral measurements, the lifetimes associated with these decays at room temperature were too short to measure reliably on the gated system and are denoted in the table with footnote *c*. At 77 K in glass, these lifetimes were 10 (593 nm) and 7.9 μs (600 nm) for **3** and **5**, respectively. Under identical conditions, we measured $[Ru(bpy)_3]^{2+}$ to be 5.1 μs (582 nm). The broad, structureless appearance of this band for **3** and **5** in the gated spectra and the similarity of these lifetimes to that of $[Ru(bpy)_3]^{2+}$ further support the assignment of this shorter wavelength component of the dual emission as ^{3}MLCT in origin. This ^{3}MLCT component does not contribute to the emission of **4** or **6** at room temperature or at 77 K, and as expected no signals were detected between 575 and 625 nm in the lifetime measurements. From this observation, it follows that 4-substitution of the pyrenylethynylene unit on the 1,10-phenanthroline ring and increased numbers of pyrenylethynylene triplets are factors that funnel excitation energy to a single emissive state of ^{3}IL character. It is tempting to look for a common photophysical phenomenon to account for the differential behavior of **4** and **6**, with respect to **3** and **5**; however, it is more likely that two different phenomena lead to the same observable outcome for **4** and **6**. This notion is supported by the drastically different ^{3}IL-based lifetimes measured for **4** and **6** at room temperature and at 77 K, whereby **4** exhibits the shortest lifetimes under all conditions and **6** exhibits the longest lifetimes under all conditions.

At room temperature, the lifetime measured at 700 nm for **4** was 22 μs, which doubled to 44 μs in glass (693 nm). These values for **6** were 270 μs (670 nm) and 3.44 ms (672 nm), respectively. The red-shifted spectra and substantially shorter lifetimes for **4** relative to those of **6** point toward different explanations for the absence of dual emission from two distinct states in these examples. The greater electronic communication between Ru(II) and the organic chromophore afforded by 4-substitution on the 1,10-phenanthroline ring in **4** may serve to spread the triplet over a very large molecular region,[8] making a highly delocalized triplet state that is lower in energy than the other dyads, including **6**. The decreased energy of this triplet would be expected to lead to more efficient nonradiative decay back to the ground state and possibly much shorter lifetimes as a consequence. This larger energy disparity between ^{3}IL and higher-lying ^{3}MLCT states might also eliminate any contribution of the latter to the thermalized excited-state emission. On the other hand, **6** has an increased number of ^{3}IL triplets relative to all of the other dyads, and others[5,26] have shown definitively in related (but not identical) systems that increasing the number of these states favors emission from these less polar configurations. Reducing the number of pyrenylethynylene-derived triplets from three (as in **6**) to one (as in **3**) decreased the lifetime of the ^{3}IL state to 240 μs (673 nm) at room temperature and to 3.43 ms in glass at 77 K. The ^{3}IL-based lifetimes measured for **3** and **6** at 77 K were within experimental error, and their lifetimes at room temperature were close enough to rule out any significant contribution from an equilibrium mixture of ^{3}MLCT and ^{3}IL-based triplets. Dyad **5** displayed lifetimes that were intermediate between **3** and **4**, and these values were 140 μs (668 nm) at room temperature and 330 μs in glass. Similarly, there was no evidence for excited-state equilibration between ^{3}MLCT and ^{3}IL states in the case of **5**.

The value 240 μs might be the longest lifetime reported for ^{3}IL phosphorescence in a Ru(II) dyad containing a single organic chromophore without a second diimine scaffold for imparting low-lying ^{3}LLCT states.[4] Because of the extreme oxygen sensitivity of excited-state lifetimes in these systems, it is possible that the lifetimes reported for other systems are actually longer, and we have certainly found this to be the case in instances where the phosphorescence lifetimes were assigned by transient absorption.[13] It should be pointed out that the long-lived excited state observed in transient absorption experiments is not always the emissive state, which may be responsible for the discrepancy in lifetimes measured for **5** by others[13] (58.4 μs) in comparison to this work (140 μs). Transient absorption determination of excited-state lifetimes would complicate the detection of dual emissive states with distinct lifetimes.

The overlapping ^{3}MLCT and ^{3}IL emissions preclude an accurate determination of radiative and nonradiative rate constants for dyads **3** and **5**. Conveniently, **4**, which is the dyad showing the most evidence for impure ^{3}IL phosphorescence, or the most ^{3}ILCT character, does not produce any trace of pure ^{3}MLCT emission under our experimental conditions. In fluid solution at room temperature, k_r and k_{nr} for **4** were calculated as 0.08×10^4 and 0.04×10^6 s^{-1}, respectively. In glass at 77 K, these values decreased to 0.07×10^4 and 0.02×10^6 s^{-1}, respectively. With the consideration that the quantum yields for ^{3}IL phosphorescence contain some contribution from ^{3}MLCT emission in the other dyads, the estimated values for k_r and k_{nr} are even smaller for these systems. Unusually small values for k_r and k_{nr} in Ru(II) coordination complexes have been attributed to pure ^{3}IL phosphorescence by others,[10] and the values calculated and estimated for this family of dyads fall well within the accepted published values for ligand-localized excited states. In the case of **6**, which displayed the smallest quantum yields and the longest lifetimes in the series at both temperatures, k_r and k_{nr} were calculated as 0.023×10^2 and 0.37×10^4 s^{-1} in fluid solution and as 0.058×10^2 and 0.029×10^4 s^{-1} in glass. These extremely low values for k_r and k_{nr} may be the smallest reported to date, and certainly the unprecedented long lifetimes and low radiative rate constants lead to phosphorescence that is acutely sensitive to trace amounts of molecular oxygen. While this sensitivity is more than a nuisance in the quantitative determination of photophysical parameters, it is a property unique to relatively few families of Ru(II)-based coordination complexes and can be exploited for photobiological applications such as in vivo luminescent oxygen sensing or in the photodynamic destruction of unwanted cells that may be compromised in oxygen tension.

3.3.4. Considerations Regarding Dual Emission. It is common to view dual emission as anomalous, but in cases where there exists poor electronic conduction between two

discrete emitting states in a single molecular structure, dual emission can be observed.[8] However, when electronic communication is facile, particularly in Ru(II)-based dyads that bear an ethynylene linker, discrete triplet emission from two distinct states is extremely rare or is at least largely unreported. It is interesting to note that the greater electronic communication between Ru(II) and the organic chromophore afforded by 4-substitution on the 1,10-phenanthroline ring in **4** eliminated any contribution from the ^{3}MLCT state to the excited-state dynamics measured over nanoseconds to milliseconds at room temperature or at 77 K. This contribution from the ^{3}MLCT was also eliminated in **6**, the homoleptic analogue of **3**, where all three coordinating ligands were grafted with pyrenylethynylene units.

When considering cases of dual emission, it is imperative to rule out the presence of a minor impurity as the source of the second emissive state. In an effort to eliminate this possibility, multiple batches of each dyad were prepared by different researchers on different scales and all samples gave identical results within experimental error. We also prepared **5** using microwave synthesis, and the contribution of the short and long components to the overall excited-state decay profiles remained unchanged. Because we also had the perdeuterated analogues of **3**−**5** on hand, we confirmed the presence of the second, weakly emissive ^{3}MLCT state in both **3** and **5**. As in the case of **4**, its bpy-d_8 counterpart did not display ^{3}MLCT on any time scale under investigation. All of the dyads were confirmed to be 99.9% pure by HPLC. To the best of our knowledge, we have ruled out the possibility that the observation of dual emission from **3** and **5** arises from minor impurities. We also note that dual emission has been observed by others in a related system at 77 K.[12]

3.3.5. Singlet Oxygen Generation. The extreme oxygen sensitivity of the photoluminescence from the ^{3}IL states of these dyads has important ramifications for the generation of singlet oxygen ($^1O_2$) and consequently those photobiological applications that rely on the production of singlet oxygen. The quantum yields for $^1O_2$ production were calculated for this series of dyads from direct measurement of $^1O_2$ emission centered at 1268 nm. $[Ru(bpy)_3]^{2+}$, with a reported $^1O_2$ quantum yield of 0.56, was used as the reference.[27] Despite their differences in emission quantum yields, lifetimes, and dual emissive profiles, **3**, **5**, and **6** produced almost identical $^1O_2$ quantum yields of 0.65, 0.68, and 0.67, respectively. On average, these dyads were approximately 20% more efficient at generating $^1O_2$ than the parent $[Ru(bpy)_3]^{2+}$ complex, and dyad **4** was >55% more efficient with its $^1O_2$ quantum yield of 0.87. This increase in $^1O_2$ generation over $[Ru(bpy)_3]^{2+}$ was not unexpected, given the much longer triplet lifetimes of **3**−**6** in deaerated acetonitrile in comparison to the parent complex.[28] While caution must be exercised in establishing structure−activity relationships within a relatively small family of complexes, the notably larger $^1O_2$ yield sensitized by **4**, despite a much shorter lifetime in deaerated acetonitrile, paralleled deviations in other photophysical properties measured for this particular dyad relative to the rest of the series. Therefore, an unusually long lifetime is not the only factor that dictates the proportion of excited-state energy that is transferred to molecular oxygen. Better matched energies between the ^{3}IL (or ^{3}IL/^{3}ILCT) state and singlet oxygen, reduced values for k_r, fundamental differences in the nature of the excited state, the redox potential of the excited state, the polarity of the local environment, and the possibility of chemical quenching of $^1O_2$ are all factors that collectively influence the predominant nonradiative decay pathway(s) for a given system.[29] Qualitatively it appears from the present investigation that once the ^{3}IL or ^{3}IL/^{3}ILCT state is established as the key excited-state determinant, further lengthening of the lifetime does not a priori result in a better singlet oxygen yield. To illustrate, the dyad with the shortest excited-state lifetime, namely **4**, was the best $^1O_2$ sensitizer in this series.

The exceptionally large $^1O_2$ quantum yields overall explain, in part, the oxygen sensitivity of the complexes and point toward a general utility as photodynamic agents in type II photoprocesses. Additional modes of quenching by oxygen are also possible, including electron transfer to form superoxide, among others, and it is anticipated that the unusually long lifetimes of the dyads must necessarily invoke more than one mechanism of excited-state deactivation. Although the exploration of these other quenching mechanisms was beyond the scope of the present investigation, in previous work[7] we have shown that the bpy-d_8 counterparts of **3** and **5** are capable of participating in oxygen-independent type I photoprocesses, and this behavior extended to the present series as well. The ability to function under hypoxic conditions is a rare phenomenon and should be considered a valuable property in photodynamic applications where oxygen levels can be highly variable and not easily predicted. To demonstrate this concept, we probed these dyads as PDT agents against in vitro metastatic melanoma, a cancer model whereby metabolic abnormalities have been reported to lead to lower oxygen saturation of hemoglobin in vivo, a clear indication of hypoxia.[30]

3.4. Photodynamic Activity. *3.4.1. Standard in Vitro PDT Assessment.* We previously reported the dark and light cytotoxicity profiles for the bpy-d_8 analogues of **3** and **5** in human leukemia cells (HL60).[7] This cell line has also been used by others[31] to probe in vitro PDT activity and provides a standard point of reference for the present series. The dark and light cytotoxicity profiles for **3**−**6** in HL60 cells are given in Table 5 along with **1** and **2** as reference complexes. Briefly, the cells were dosed with photosensitizer concentrations of 1 nM to 300 μM (300 μM was the upper limit in this family due to solubility constraints) and allowed to incubate for 1 h, a notably short drug-to-light interval, before 100 J cm^{-2} of visible light was delivered. After PDT treatment, the cells were incubated for another 72 h (Alamar Blue added at 48 h) and counted. Structures **1** and **2** (Chart 1) contain hydrogen or a phenyl group in the place of pyrene, respectively, and serve to

Table 5. Photobiological Activity of Dyads 3−6, Reference Metal Complexes 1 and 2, and Cisplatin in HL60 Cells with (100 J cm^{-2} White Light) and without Light Treatment[a]

	EC_{50} (μM)		
compd	dark	light (100 J cm^{-2})	photocytotoxicity index (PI)
1	209	43	4.9
2	73	10	7.3
3	262	0.15	1747
4	84	0.22	382
5	187	1.8	104
6	245	42	5.8
cisplatin	25	25	1

[a]PI is the ratio of dark to light toxicity and reflects the effective PDT range of the PS. Cisplatin is not a PS; it is a well-known clinical agent and serves as both a control and a reference.

dx.doi.org/10.1021/ja408426z | J. Am. Chem. Soc. 2013, 135, 17161−17175

underscore the importance of the pyrene unit for potent photobiological activity. For example, **1** displayed a light EC_{50} value of 43 μM, almost 300 times less potent than the best agent in the series, and **2** was less active by approximately 70-fold. Strikingly, light activation of dyads **3** and **4** occurred in the nanomolar regime, with **3** being slightly more phototoxic than **4** (EC_{50} = 150 vs 220 nM). Their dark toxicities were comparatively low, but **3** exhibited less toxicity with a dark EC_{50} of over 260 μM. The high light toxicity of **3** combined with its low dark toxicity gave a PI of more than 1700, which is 1 order of magnitude greater than the largest reported values measured with much longer drug-to-light intervals.[31] The potential therapeutic window for **4** was slightly less, with a PI of approximately 380, but still larger than the best agents to date. **5**, in contrast, was less impressive but as good as the best reported agents (light EC_{50} = 1.8 μM, PI > 100). We also measured the photocytotoxicity responses for **3**−**5** at lower doses of visible light (down to 5 J cm^{-2}), and the light EC_{50} values decreased accordingly but remained in the 500 nM to 1.5 μM regime. The data collected for **6** are included in the table for completeness, but its insolubility in aqueous media precluded an accurate determination of its in vitro PDT against HL60 cells, and so it was not thoroughly investigated at other light doses or in additional cell lines. As speculated in the Introduction, inclusion of two or three pyrenyl units was sufficient to cause the chloride salt to precipitate in water, and this problem was exacerbated in buffered solutions.

The light-activated form of these agents was up to 170 times more toxic than cisplatin, arguably the most prescribed anticancer agent in the clinic, under our conditions. The activity of cisplatin reported by Glazer et al. was 3.1 μM in HL60 cells, indicating that the present series might compare even more favorably to the Ru(II)-based DNA photobinding agents and cisplatin. Notably, these dyads were up to 10 times less toxic (dark EC_{50}) than cisplatin measured under our conditions and approximately 85 times less toxic than cisplatin measured using conditions reported by others.[31,32] Any agent that can outperform cisplatin and selectively target cells exposed to light while maintaining low systemic toxicity makes a very attractive alternative to conventional chemotherapeutic agents that exhibit high general toxicity. As reported for the strained Ru(II) DNA photobinding agents, the phototoxic Ru(II) dyads annihilated 100% of the cancer cell population, a desired property that has posed a challenge for light-activated agents.[31] Possible advantages that the Ru(II) dyads have to offer are that they appear to be significantly more potent upon light activation relative to other systems and exhibit long-term photostability in the formulating solution under ambient lighting. A perceived drawback associated with this specific family of dyads is that its members display very weak absorption of light in the PDT window, which could limit the utility of these first-generation derivatives to noninvasive, accessible tumors or microbial sterilization applications. Nevertheless, the potency of these dyads under a vast range of oxygen tension resulting from the novel exploitation of ^{3}IL excited states for metal−organic PDT warrants further the investigation of these dyads in combination with optimized light sources and protocols as well as of second-generation, red-shifted dyads for use in challenging cancer models such as malignant melanoma.

3.4.2. Melanoma as an Attractive PDT Target. Despite the common misconception that malignant melanoma is a relatively innocuous skin cancer, the prognosis for metastatic melanoma is poor. Early detection of localized melanoma can be addressed by surgical resection, but there exists no curative therapy for metastatic melanoma or melanoma with metastatic potential.[33] Additionally, the recurrence rate for resected melanoma is relatively high. The median survival time for patients with stage IV melanoma is approximately 9 months, and 3 year survival rates are less than 15%.[2,34] These grim statistics derive, in large part, from the fact that melanocytes are not susceptible to the traditional arsenal of anticancer approaches because they are well-equipped to combat a broad spectrum of xenobiotics, reactive oxygen species (ROS), and ultraviolet and ionizing radiation.[35] They have evolved, in fact, to serve as the first line of defense against harmful UV radiation from the sun and other damaging environmental agents. Causes of therapeutic resistance in melanoma stem from a number of diverse mechanisms, which include (i) increased DNA repair in response to DNA-damaging agents, (ii) overexpressed antiapoptotic proteins such as Bcl-2, (iii) altered expression of oncogenes such as RAS and BRAF or the tumor suppressor p53, and (iv) methylation-mediated silencing of the APAF-1 gene.[36] However, these more general mechanisms of resistance do not account for the fact that melanomas are particularly insensitive to chemotherapeutic and radiation regimens in comparison to the broad spectrum of nonmelanoma cancers. One plausible explanation for this difference can be attributed to a lysosome-related organelle in melanocytes, termed the melanosome, which is unique to melanocytes and is specialized for the production of melanin. The melanosome possibly arms melanomas with additional mechanisms of resistance that relate to drug sequestration and export, and melanin itself has been shown to act as an intracellular antioxidant, detoxifying chemotherapeutically generated ROS.[2,37] It is well-known that melanomas present intrinsic multidrug resistance (MDR), expressing a host of ABC transporters (ABCA9, ABCB1, ABCB5, ABCB8, ABCC1, ABCC2, and ABCD1) that efflux both anticancer drugs and toxic melanin intermediates and metabolites from melanoma cells.

Due to the uncanny ability of melanoma cells to outsmart conventional chemotherapeutic regimens, immunotherapy (e.g., Ipilimumab, an effector of CTLA-4) and targeted therapy (e.g.,Vemurafenib, a BRAF inhibitor) broadly represent the direction of advanced melanoma treatment. Unfortunately, these therapies are not curative and prolong survival often by months, not years. Almost half of all melanoma patients will not test positive for the BRAF gene mutation,[38] and patients with unrelated autoimmune disorders will not be candidates for immunotherapy.[39] Clearly, alternate strategies are needed, and PDT, as an example, has produced encouraging results in a variety of different in vitro and in vivo experimental models[33] as well as in several clinical reports.[2] These sporadic reports, while promising, have not been followed up by extensive clinical studies using select photosensitizers and specialized PDT protocols. Rather, they have employed traditional type II, clinically approved photosensitizers that have led to PDT-induced pigmentation and increased SOD activity (antioxidant defense) in some cases. While this PDT-triggered response in melanoma is far from understood, it may be responsible for the documented resistance of pigmented melonomas to PDT in comparison to amelanotic melanomas[2,40] and a general reluctance to consider PDT as a viable adjuvant therapy in advanced melanoma treatment. We hypothesize that new photosensitizers capable of generating an acute burst of ROS and other phototoxins at the site of the melanosome—even

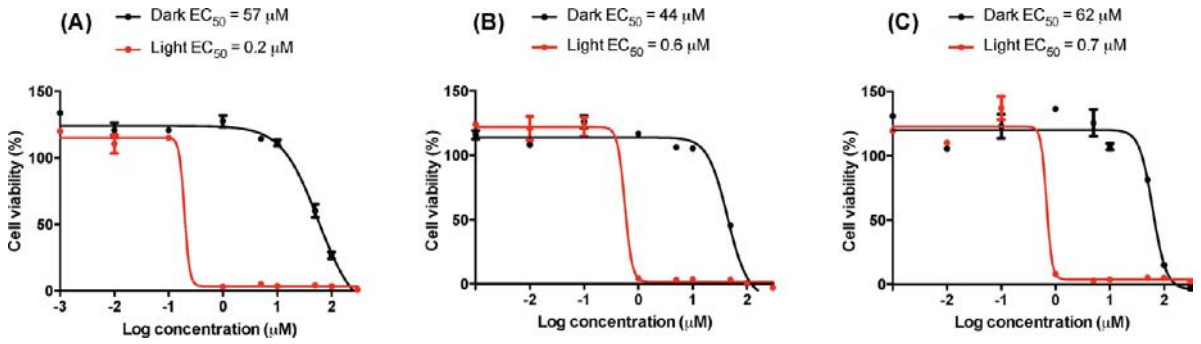

Figure 4. In vitro PDT dose–response curves for **3** (a), **4** (b), and **5** (c) in Malme-3M cells. Dark (black) and light (red) conditions were identical except that the PDT-treated samples were irradiated with visible light for 15 min (7 J cm^{-2}).

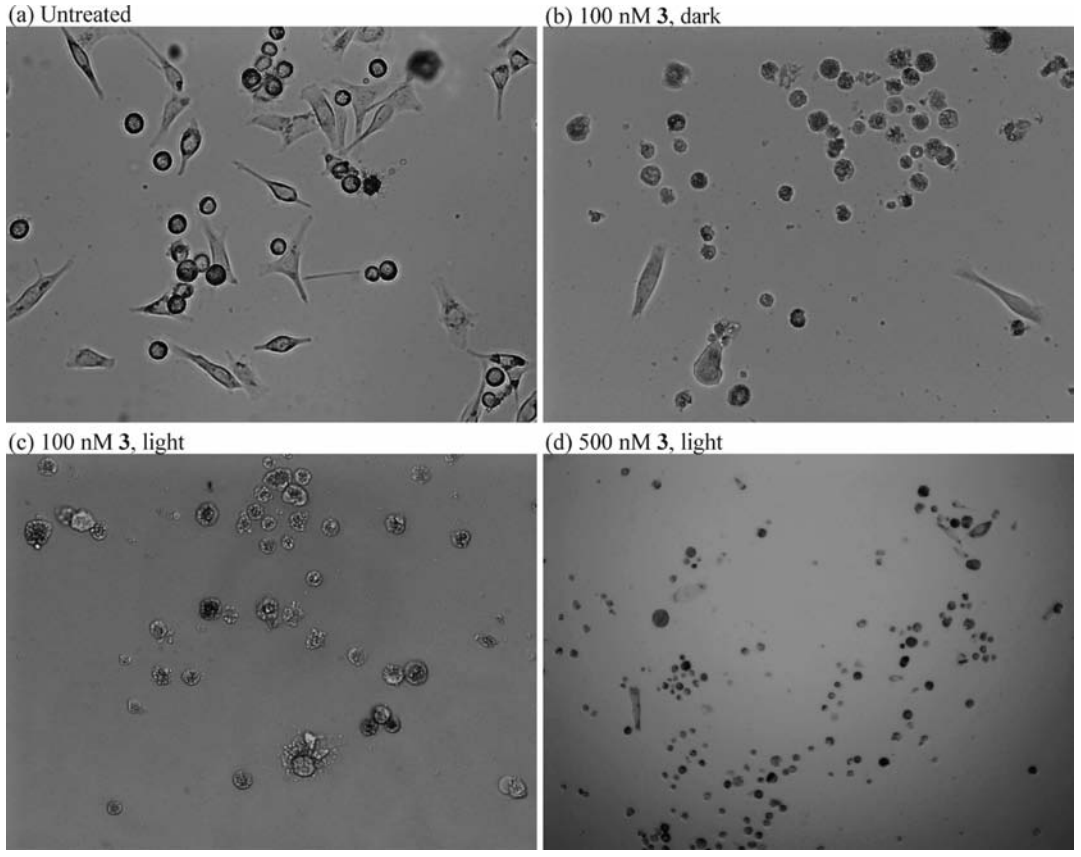

Figure 5. Malme-3M cells untreated (a) and treated with **3** in the dark (b) and with visible light (c, d) observed by bright-field imaging at 150× magnification. Light-treated samples were illuminated for 15 min with visible light (7 J cm^{-2}) and imaged at 72 h postirradiation.

under hypoxia (pO_2 <2%)[41,42]—will destroy pigmented and unpigmented melanocytes alike and be well-poised for further development as a new tool in melanoma treatment. The dyads presented in this study are attractive candidates for this purpose, given their modularity for further optimization, susceptibility to excited-state quenching even in the absence of oxygen, and ability to elicit extensive photodamage to nucleic acids, proteins, and lipids in hypoxia.

3.4.3. In Vitro PDT in a Metastatic Melanoma Model. The Malme-3M cell line was used as an in vitro model of metastatic melanoma. These cells are human fibroblasts isolated from a malignant melanoma lung metastasis in a 43-year-old Caucasian male. They grow as a mixture of suspension and adherent cells and form pigmented melanoma in nude mice (ATCC HTB-64). Malme-3M is one of the cell lines included in the NCI-60 panel and has been widely utilized for drug screening and molecular target identification. In our experiments, Malme-3M cells were dosed with 1 nM to 300 μM of dyads **3**–**5** and incubated for 1 h prior to PDT treatment with a low dose of 7 J cm^{-2} of visible light. The cell–photosensitizer samples were treated with a range of light doses, but we chose to include the low-dose data to highlight the nanomolar activity against metastatic melanoma cells with minimal light treatment. The treated cells were incubated for an additional 72 h and then counted.

Dose–response profiles for in vitro PDT delivered to Malme-3M cells were similar for dyads **3**–**5** (Figure 4). The dark toxicities of these dyads ranged from an EC_{50} value of 44 μM for **4** to 62 μM for **5** with **3** between at 57 μM. The higher overall dark toxicity of the dyads toward Malme-3M cells over

dx.doi.org/10.1021/ja408426z | J. Am. Chem. Soc. 2013, 135, 17161–17175

other cancer cell lines (up to 5 times more toxic in some cases) points toward a potential selectivity against melanoma, although this assertion is grossly premature. Nevertheless, significant morphological changes to the Malme-3M cells were discernible when they were treated with as low as 100 nM of the dyads in the dark (Figure 5b). These changes in phenotype were not observed for dyad-treated HL60 cells in the dark up to 50−100 μM. The light toxicities for **3**−**5** exhibited more variation, with **3** yielding a light EC_{50} of 200 nM under a very low dose of visible illumination. Complexes **4** and **5** gave correspondingly potent PDT with EC_{50} values of 600−700 nM, respectively. The cell morphological changes produced by light activation of **3** are highlighted in Figure 5 with 100 nM (c) and 500 nM (d) **3**. It is notable, from a selectivity perspective, that collectively the dyads gave submicromolar PDT at a very low light dose, 20 times less than what produced the data reported in Table 5 for HL60 cells. However, more impressive and surprising is the fact that the light-activated potency of **3**−**5** is of this magnitude in *pigmented* melanoma cells, which are believed to be inherently less susceptible to PDT in comparison to amelanotic melanoma cells or other cancer cells in general.[2,33] Active melanin production by melanosomes of the pigmented Malme-3M cell line was verified using bright-field optical microscopy as darkened regions in the image (Figure 6).[43] Accumulation of a PS in the melanosomes might trigger

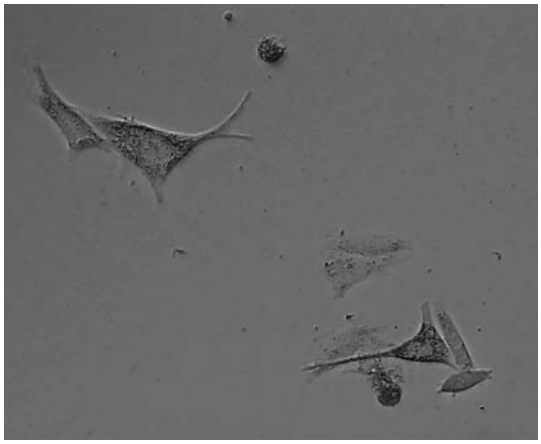

Figure 6. Malme-3M cells showing active melanin production by melanosomes as darkened regions in the bright-field image at 150× magnification (zoomed image).

the destruction of these organelles, initiating the release of cytotoxic melanogenesis intermediates and byproducts, including H_2O_2 and highly reactive quinones, that result in cell death.[2,33] It is unclear whether dyads **3**−**5** are capable of damaging the melanosome, a strategy that researchers feel is the best way to target melanoma cells due to their propensity to both destroy and efflux drugs effectively, but a more detailed study is currently underway. Regardless, this preliminary account clearly establishes the ability of blue-green absorbing photosensitizers to completely destroy pigmented metastatic melanoma cells at submicromolar concentrations and thus provides a compelling argument for revisiting the idea of developing PDT as an alternate strategy in the treatment of melanoma.

3.4.4. Conclusions Regarding Structure−Activity Relationships. Within this small family of Ru(II) dyads, the photobiological activity documented in HL60 cells or in Malme-3M cells could not be directly correlated to differences in singlet oxygen yields, emission quantum yields or lifetimes, visible-light absorption cross sections, absorption or emission wavelength maxima, or radiative and nonradiative rate constants. To illustrate this point, **4** had the shortest lifetime, the largest $^1O_2$ quantum yield, and the most red-shifted absorption and emission profiles in the series, yet its activity in both HL60 and Malme-3M cells was intermediate between those of **3** and **5**. However, in the single comparison between **3** and **5**, **3** was more potent in both cell lines with a much larger PI in both cases. The excited-state lifetime of **3** was 70% longer than that measured for **5**, its singlet oxygen quantum yield was roughly the same, and its ex vitro binding affinity for DNA was 3.5 times lower. Other factors are certainly at play in vitro, including differences in cellular uptake and efflux, subcellular localization, biological targets, mechanism of action, and metabolism. Nevertheless, it was apparent that the pyrenylethynylene unit is crucial for nanomolar light toxicity, given that the best activity from **1** or **2** gave an EC_{50} value of 10 μM and PI of 7.3 with 100 J cm^{-2} of visible irradiation, hardly impressive activity. Importantly, nanomolar PDT in both cell lines, particularly in the reportedly more resistant Malme-3M line, was observed regardless of the substitution profile of the pyrenylethynylene group, despite the fact that the photophysical properties of the dyads, especially of **4** relative to **3** and **5**, were substantially different. Because other DNA-binding, Ru(II)-based complexes containing the pyrene chromophore display lowest-lying ^{3}MLCT excited states of relatively short duration[4] and do not result in comparable photobiological activity under our conditions, the existence of low-lying ^{3}IL states is inferred to be a major determinant in the potent photobiological activity of this series rather than the DNA-intercalating ability or the lipophilic properties of pyrene itself. In other words, we conclude that the dramatic phototoxicity of these dyads toward cancer cells stems from their extraordinary excited-state quenching profiles combined with a lipophilic handle that can also intercalate DNA or localize in other hydrophobic regions. The generality of this approach, using ^{3}IL states for metal−organic PDT, is demonstrated by the tolerance of the photobiological activities to changes in substitution pattern that produce correspondingly larger changes in excited-state lifetimes but maintain lowest lying ^{3}IL states that are extremely sensitive to trace amounts of oxygen. This potency is likely not limited to ^{3}IL states but should be attainable in other situations where configuration mixing or excited-state equilibration[10] leads to large excited-state quenching constants with very low radiative rates.

4. CONCLUDING REMARKS

Dyads that differ in the number of appended ethynylpyrenyl units might be expected to exhibit quantitative differences in their spectroscopic properties if the number density of pyrene chromophores shifts the excited-state equilibrium toward pyrene-based IL triplets in a ^{3}MLCT−^{3}IL mixture. However, **3** and its homoleptic analogue **6** displayed similar photophysical properties, substantiating the assertion that the excited-state dynamics in these systems are dominated by lowest-lying ^{3}IL states rather than equilibrium mixtures of MLCT and IL triplets. This observation was particularly noteworthy in that the 2,2′-bipyridine (bpy) analogue of **5**, where the ethynylpyrenyl unit is grafted to position 5 of a bpy ring, displays a lifetime of 42 μs and a photophysical profile consistent with a ^{3}MLCT-based excited state that is in equilibrium with the IL

dx.doi.org/10.1021/ja408426z | J. Am. Chem. Soc. 2013, 135, 17161−17175

ethynylpyrenyl-localized triplet.[26] This equilibrium distribution can be shifted systematically to pure ^{3}IL- or ^{3}ILCT-based phosphorescence in the corresponding bis- and tris-pyrenylethynylene complexes.[10] In terms of spatial orientation, C5 on bpy is analogous to C3 on 1,10-phenanthroline, but the two core diimine ligands lead to markedly different photophysical behavior in the dyads whereby one ethynylpyrenyl-fused diimine ligand is sufficient for pure ^{3}IL-based phosphorescence in the case of phen. Therefore, the identity of the diimine ligand bearing the organic chromophore imparting relatively low lying $\pi\pi^*$ triplets plays an important role in determining whether these resulting ^{3}IL states will dictate the ensuing excited-state dynamics and whether the emissive states will be "pure" or constitute an equilibrium mixture with ^{3}MLCT states.

Within the spectrum of accessible ligand-localized triplets, one can envision a continuum of "purity" associated with these ^{3}IL states that ranges from being relatively nonpolar and localized to pyrene ($^3\pi\pi^*$) to exhibiting some amount of charge transfer between the pyrene or ethynylpyrene and the diimine ligand (^{3}ILCT), although the latter is slight in comparison to formal ^{3}MLCT states that characterize traditional Ru(II) photophysics. This fine tuning within ^{3}IL states is demonstrated nicely in the present dyad series, where ordering by the calculated thermally induced Stokes shifts places **6** as the least polar state and **4** as the state having the most charge-transfer character. **3** and **5** are similar, but **5** is slightly more polarized. The ^{3}IL-based lifetimes measured at room temperature and at 77 K also reflect this notion in that **6** possesses the longest luminescence lifetime and **4** displays the shortest. In agreement with their thermally induced Stokes shifts, the lifetime of **5** is shorter than that measured for **3**.

In the present family of dyads, the long-lived ^{3}IL-based phosphorescence can be tuned from 22 to 270 μs in fluid solution and from 44 to 3440 μs in a solid matrix on the basis of the number and positioning of pyrenylethynylene units in the complexes. While the photophysical properties are affected significantly by these minor structural modifications, the photobiological potency remains high, in the submicromolar regime even at very short drug-to-light intervals, for all of the dyads. This unprecedented potency is sufficient to destroy even those cells that are notoriously resistant to traditional chemotherapeutics, and the present work applies this concept to an in vitro model of metastatic melanoma, a form of cancer that is particularly aggressive and in need of new treatment strategies. The modular nature of these Ru(II)-based transition-metal complexes are particularly well-suited for further optimization, including broadening the wavelengths that can be used for activation as well as controlling oxygen-independent versus oxygen-dependent partitioning of photoreactivity. Current efforts are underway to demonstrate the incredible breadth of tunability in these two specific areas and will be reported separately.

■ ASSOCIATED CONTENT

Ⓢ Supporting Information

Figures giving ^{1}H NMR spectra for ligands **5-BEP** and **4-PEP** and complexes **1**–**6** as well as absorption and emission spectra for **3**–**6** at 77 K and at room temperature. This material is available free of charge via the Internet at http://pubs.acs.org.

■ AUTHOR INFORMATION

Corresponding Authors

E-mail for S.A.M.: sherri.mcfarland@acadiau.ca.

E-mail for R.P.T.: thummel@uh.edu.

Notes

The authors declare no competing financial interest.

■ ACKNOWLEDGMENTS

S.A.M., R.L., S.M., H.Y., M.S., and R.H. thank the Canadian Institutes of Health Research, the Natural Sciences and Engineering Research Council of Canada, the Canadian Foundation for Innovation, and the Nova Scotia Research and Innovation Trust for financial support and Prof. Todd Smith for use of his cell and tissue culture facility. R.P.T., L.K., R.Z., A.C., and C.D. thank the Robert A. Welch Foundation (E-621) and the National Science Foundation (CHE-0714751) for financial support of this work. We also thank Prof. Steven F. Morris, MD, Head of the Multidisciplinary Melanoma Clinic (QEII Health Sciences Centre, Halifax, NS), for his careful review and insightful comments regarding the biological aspects and clinical relevance of this manuscript.

■ REFERENCES

(1) Plaetzer, K.; Krammer, B.; Berlanda, J.; Berr, F.; Kiesslich, T. *Lasers Med. Sci.* **2009**, *24*, 259–268.
(2) Baldea, I.; Filip, A. G. *J. Physiol. Pharmacol.* **2012**, *63*, 109–118.
(3) Juris, A.; Balzani, V.; Barigelletti, F.; Campagna, S.; Belser, P.; von Zelewsky, A. *Coord. Chem. Rev.* **1988**, *84*, 85–277.
(4) McClenaghan, N. D.; Leydet, Y.; Maubert, B.; Indelli, M. T.; Campagna, S. *Coord. Chem. Rev.* **2005**, *249*, 1336–1350.
(5) Kozlov, D. V.; Tyson, D. S.; Goze, C.; Ziessel, R.; Castellano, F. N. *Inorg. Chem.* **2004**, *43*, 6083–6092.
(6) Simon, J. A.; Curry, S. L.; Schmehl, R. H.; Schatz, T. R.; Piotrowiak, P.; Jin, X.; Thummel, R. P. *J. Am. Chem. Soc.* **1997**, *119*, 11012–11022.
(7) Monro, S.; Scott, J.; Chouai, A.; Lincoln, R.; Zong, R.; Thummel, R. P.; McFarland, S. A. *Inorg. Chem.* **2010**, *49*, 2889–2900.
(8) Harriman, A.; Khatyr, A.; Ziessel, R. *Dalton Trans.* **2003**, 2061–2068.
(9) Ford, W. E.; Rodgers, M. A. J. *J. Phys. Chem.* **1992**, *96*, 2917–2920.
(10) Goze, C.; Kozlov, D. V.; Tyson, D. S.; Ziessel, R.; Castellano, F. N. *New J. Chem.* **2003**, *27*, 1679–1683.
(11) Harriman, A.; Hissler, M.; Khatyr, A.; Ziessel, R. *Chem. Commun.* **1999**, 735–736.
(12) Tyson, D. S.; Henbest, K. B.; Bialecki, J.; Castellano, F. N. *J. Phys. Chem. A* **2001**, *105*, 8154–8161.
(13) Ji, S.; Wu, W.; Wu, W.; Song, P.; Han, K.; Wang, Z.; Liu, S.; Guo, H.; Zhao, J. *J. Mater. Chem.* **2010**, *20*, 1953–1963.
(14) Brozyna, A. A.; VanMiddlesworth, L.; Slominski, A. T. *Int. J. Cancer* **2008**, *123*, 1448–1456.
(15) Case, F. H. *J. Org. Chem.* **1951**, *16*, 1541–1545.
(16) Hissler, M.; Connick, W. B.; Geiger, D. K.; McGarrah, J. E.; Lipa, D.; Lachicotte, R. J.; Eisenberg, R. *Inorg. Chem.* **2000**, *39*, 447–457.
(17) Ziessel, R.; Suffert, J.; Youinou, M.-T. *J. Org. Chem.* **1996**, *61*, 6535–6546.
(18) Duliere, E.; Devillers, M.; Marchand-Brynaert, J. *Organometallics* **2003**, *22*, 804–811.
(19) Sullivan, B. P.; Salmon, D. J.; Meyer, T. J. *Inorg. Chem.* **1978**, *17*, 3334–3341.
(20) Galoppini, E.; Guo, W.; Zhang, W.; Hoertz, P. G.; Qu, P.; Meyer, G. J. *J. Am. Chem. Soc.* **2002**, *124*, 7801–7811.
(21) Glazer, E. C.; Magde, D.; Tor, Y. *J. Am. Chem. Soc.* **2007**, *129*, 8544–8551.
(22) Zong, R.; Wang, B.; Thummel, R. P. *Inorg. Chem.* **2012**, *51*, 3179–3185.
(23) Abdel-Shafi, A. A.; Beer, P. D.; Mortimer, R. J.; Wilkinson, F. *Phys. Chem. Chem. Phys.* **2000**, *2*, 3137–3144.

(24) Shiotsuka, M.; Tsuji, Y.; Keyaki, K.; Nozaki, K. *Inorg. Chem.* **2010**, *49*, 4186−4193.
(25) Orellana, G.; Alvarez Ibarra, C.; Santoro, J. *Inorg. Chem.* **1988**, *27*, 1025−1030.
(26) Hissler, M.; Harriman, A.; Khatyr, A.; Ziessel, R. *Chem. Eur. J.* **1999**, *5*, 3366−3381.
(27) DeRosa, M. C.; Crutchley, R. J. *Coord. Chem. Rev.* **2002**, *233/234*, 351−371.
(28) Abdel-Shafi, A. A.; Worrall, D. R.; Ershov, A. Y. *Dalton Trans.* **2004**, 30−36.
(29) Wilkinson, F. *Pure Appl. Chem.* **1997**, *69*, 851−856.
(30) Cotran, R. S.; Kumar, V.; Collins, T. *Robbins Pathologic Basis of Disease*, 6th ed.; W. B. Saunders: Philadelphia, PA, 1999.
(31) Howerton, B. S.; Heidary, D. K.; Glazer, E. C. *J. Am. Chem. Soc.* **2012**, *134*, 8324−8327.
(32) Wachter, E.; Heidary, D. K.; Howerton, B. S.; Parkin, S.; Glazer, E. C. *Chem. Commun.* **2012**, *48*, 9649−9651.
(33) Davids, L. M.; Kleemann, B. *Cancer Treat. Rev.* **2011**, *37*, 465−475.
(34) Balch, C. M.; Gershenwald, J. E.; Soong, S. J. *J. Clin. Oncol.* **2009**, *27*, 6199−6206.
(35) Zbytek, B.; Carlson, J. A.; Granese, J.; Ross, J.; Mihm, M. C.; Slominski, A. *Expert Rev. Dermatol.* **2008**, *3*, 569−585.
(36) Chen, K. G.; Valencia, J. C.; Gillet, J.-P.; Hearing, V. J.; Gottesman, M. M. *Pigment Cell Melanoma Res.* **2009**, *22*, 740−749.
(37) Mroz, P.; Huang, Y.-Y.; Szokalska, A.; Zhiyentayev, T.; Janjua, S.; Nifli, A.-P.; Sherwood, M. E.; Ruzié, C.; Borbas, K. E.; Fan, D.; Krayer, M.; Balasubramanian, T.; Yang, E.; Kee, H. L.; Kirmaier, C.; Diers, J. R.; Bocian, D. F.; Holten, D.; Lindsey, J. S.; Hamblin, M. R. *FASEB J.* **2010**, *24*, 3160−3170.
(38) Wellbrock, C.; Hurlstone, A. *Biochem. Pharmacol.* **2010**, *80*, 561−567.
(39) Dickman, A.; Kerr, D. *Drugs in Cancer Care*; Oxford University Press: Oxford, U.K., 2013.
(40) Nelson, J. S.; McCullough, J. L.; Berns, M. W. *J. Natl. Cancer Inst.* **1988**, *80*, 56−60.
(41) Brurberg, K. G.; Thuen, M.; Ruud, E.-B. M.; Rofstad, E. K. *Radiat. Res.* **2006**, *165*, 16−25.
(42) Juzeniene, A.; Nielsen, K. P.; Moan, J. *J. Environ. Pathol. Toxicol. Oncol.* **2006**, *25*, 7−28.
(43) Palmisano, I.; Bagnato, P.; Innamorati, G.; Rotondo, G.; Altimare, D.; Venturi, C.; Sviderskaya, V.; Piccirillo, R.; Coppola, M.; Marigo, V.; Incerti, B.; Ballabio, A.; Surace, E. M.; Tacchetti, C.; Bennett, D. C.; Schiaffino, M. V. *Hum. Mol. Genet.* **2008**, *17*, 3487−3501.